

See discussions, stats, and author profiles for this publication at: <https://www.researchgate.net/publication/5233506>

# Head-to-Tail Interactions in Tyrosine/Benzophenone Dyads in the Ground and the Excited State: NMR and Laser Flash Photolysis Studies

ARTICLE in CHEMISTRY - A EUROPEAN JOURNAL · AUGUST 2008

Impact Factor: 5.73 · DOI: 10.1002/chem.200800315 · Source: PubMed

CITATIONS

12

READS

25

9 AUTHORS, INCLUDING:



Gerald Hörner

Technische Universität Berlin

22 PUBLICATIONS 128 CITATIONS

SEE PROFILE



Piotr Filipiak

Adam Mickiewicz University

18 PUBLICATIONS 165 CITATIONS

SEE PROFILE



Walter Bauer

Friedrich-Alexander-University of Erlangen-N...

154 PUBLICATIONS 3,649 CITATIONS

SEE PROFILE



Tomasz Pedzinski

Adam Mickiewicz University

36 PUBLICATIONS 149 CITATIONS

SEE PROFILE

# Head-to-Tail Interactions in Tyrosine/Benzophenone Dyads in the Ground and the Excited State: NMR and Laser Flash Photolysis Studies

Gerald Hörner,<sup>\*,[a, b]</sup> Gordon L. Hug,<sup>[a, c]</sup> Dariusz Pogocki,<sup>[d]</sup> Piotr Filipiak,<sup>[a]</sup> Walter Bauer,<sup>[e]</sup> Andreas Grohmann,<sup>[f]</sup> Anica Lämmermann,<sup>[a]</sup> Tomasz Pedzinski,<sup>[a]</sup> and Bronislaw Marciniak<sup>[a]</sup>

**Abstract:** The formation of head-to-tail contacts in de novo synthesized benzophenone/tyrosine dyads, bpUTyr, was probed in the ground and excited triplet state by NMR techniques and laser flash photolysis, respectively. The high affinity of triplet-excited ketones towards phenols was used to trace the geometric demands for high reactivity in the excited state. A retardation effect on the rates with increasing hydrogen-bond-acceptor ability of the solvent is correlated with ground-state masking of the phenol. In a given sol-

vent the efficiencies of the intramolecular hydrogen-atom-transfer reaction depend strongly on the properties of the linker: rate constants for the intramolecular quenching of the triplet state cover the range of  $10^5$  to  $10^8$  s<sup>-1</sup>. The observed order of reactivity correlates to a) the probability of close contacts (from molecular-dynamics simulations)

**Keywords:** ketones • peptides • photochemistry • pi interactions • tyrosine

and b) the extent of the electronic overlap between the  $\pi$  systems of the donor and acceptor moieties (from NMR). A broad survey of the NMR spectra in nine different solvents showed that head-to-tail interactions between the aromatic moieties of the bpUTyr dyads already exist in the ground state. Favourable aromatic-aromatic interactions in the ground state appear to correspond to high excited-state reactivity.

## Introduction

Radical centers in proteins have gained considerable interest in the past decades due to their roles as functional units or as mediators of pathological pathways. In particular, the tyrosyl radicals, Tyr(O<sup>•</sup>), as the main oxidation product of tyrosine after formal loss of one hydrogen atom, have been identified to be an integral cofactor of enzyme activity.<sup>[1]</sup>

The radical chemistry of the underlying phenol moiety of Tyr was and is the subject of intense research activity.<sup>[2]</sup>

One well-established path giving Tyr(O<sup>•</sup>) radicals in vitro is based on photoinduced reactions between tyrosine and aromatic ketones. Triplet-excited ketones are biradicaloid in nature and, thus, share many reactivity characteristics with the alkoxy radicals.<sup>[3]</sup> Numerous studies identify H-atom transfer between the phenol and the triplet state as the

[a] Dr. G. Hörner, Dr. G. L. Hug, Dr. P. Filipiak, Dipl.-Chem. A. Lämmermann, Dr. T. Pedzinski, Prof. B. Marciniak  
Faculty of Chemistry, Adam Mickiewicz University Poznan  
Grunwaldzka 6, 60-780 Poznan (Poland)  
Fax: (+48) 61-829-4367  
E-mail: hoerner@amu.edu.pl


[b] Dr. G. Hörner  
Interdisciplinary Group Time Resolved Spectroscopy  
University of Leipzig, Permoserstrasse 15  
04303 Leipzig (Germany)

[c] Dr. G. L. Hug  
Radiation Laboratory, University of Notre Dame  
Notre Dame, IN 46556 (USA)

[d] Prof. D. Pogocki  
Faculty of Chemistry, Rzeszow University of Technology  
35-959 Rzeszow (Poland)  
and  
Institute of Nuclear Chemistry and Technology  
03-195 Warszawa (Poland)

[e] Prof. W. Bauer  
Institute of Organic Chemistry  
University of Erlangen-Nürnberg  
91056 Erlangen (Germany)

[f] Prof. A. Grohmann  
Institute of Chemistry, Technical University Berlin  
10623 Berlin (Germany)

 Supporting information for this article is available on the WWW under <http://dx.doi.org/10.1002/chem.200800315> or from the author.

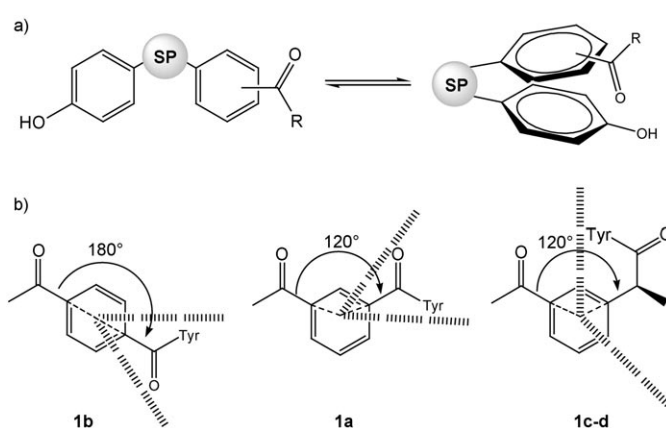
dominate quenching process in mono- and bimolecular systems.<sup>[4–7]</sup> Irrespective of the electronic nature of the lowest excited triplet state ( $n \rightarrow \pi^*$  vs  $\pi \rightarrow \pi^*$ ), H-atom transfer from phenols occurs with high efficiency (usually close to unity) and at much higher rates than observed for aliphatic alcohols. High efficiency of radical intermediate formation is usually contrasted by very inefficient product formation.<sup>[4]</sup> Thus, the excited-state energy is dissipated through consecutive H-atom-transfer steps that regenerate the starting material in the electronic ground state.<sup>[8]</sup> We used the high affinity of phenols towards triplet-excited ketones to trace the steric demands of the formation of reactive conformations in peptide-linked benzophenone/Tyr dyads.

The mechanism of the H-atom-transfer quenching of aromatic triplet states by phenols is dependent on the medium. Clear evidence for an electron-transfer-initiated two-step process is limited to aqueous media.<sup>[9]</sup> For organic media, the mechanism is interpreted in terms of a proton-coupled electron transfer.<sup>[7a]</sup> Importantly, the involvement of charge-transfer (CT) complexes or exciplexes in H-atom-transfer reactions has been invoked in several studies concerned with bi- and monomolecular ketone/phenol systems.<sup>[5b,d,7d]</sup> In a recent example, the formation of encounter complexes between the phenol and the excited ketone benzoylthiophene with a  $\pi \rightarrow \pi^*$  lowest triplet has been concluded from non-linear Stern–Volmer plots and DFT calculations.<sup>[6b,c]</sup>

Our interest in this topic began with the question of whether, and if so, how the accessible conformational space in ketone/phenol dyads could be modulated by tuning the flexibility and directionality of the linkage between the interacting groups in the ground state and in the excited state. The few studies dealing with the effect of steric constraints on monomolecular reaction rates in the ketone/phenol system revealed remarkable effects of substitution geometry on quenching rates.<sup>[5c,d,6d]</sup> In addition, significant stereoselectivity<sup>[6a,c]</sup> of the quenching process has been reported for monomolecular quenching of ketone triplets by phenols covalently linked by flexible spacers. Such constellations were shown to allow the approach of the interacting groups on a time scale much faster than the H-atom transfer itself.<sup>[5a,b]</sup>

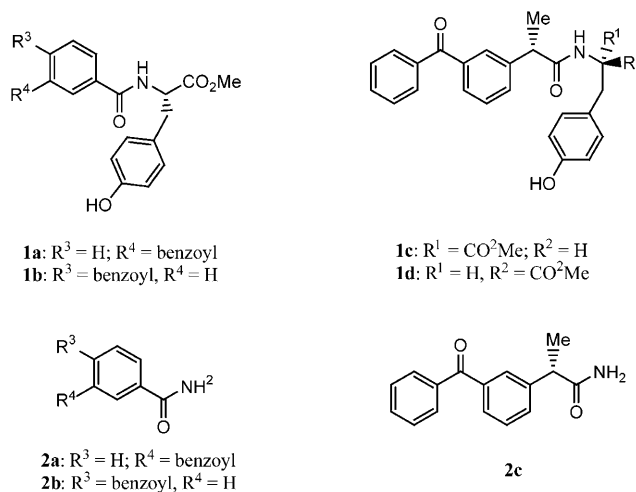
Both the formation of intramolecular complexes and the H-atom-transfer step itself require close contacts between the remote aromatic moieties (Scheme 1a). We show that the ease of formation of head-to-tail conformations in benzophenone/tyrosine, bpTyr, dyads is affected by the molecular structure, that is, by the relative orientation and the distance between the reacting moieties, and the nature of the spacer **SP**. The question arising is whether steric conditions that are favourable for electronic overlap of the reacting partners in the excited state can be probed by ground-state interactions between the remote aromatic moieties also in the ground state. The effects of molecular geometry on the ground-state conformations and on the rates and efficiencies of the intramolecular triplet quenching in ketone/phenol dyads are compared.

We used the four dyads **1a–d**, bpTyr, which were synthesized de novo from three benzophenone (bp) carboxylic



Scheme 1. a) Folding of the dyads and b) steric constraints of substitution.

acids and (*S*)- and (*R*)-tyrosine methylester, Tyr-OMe. The flexibility of the alkyl linkage is tuned by the relative position and orientation of a rigid amide bond between the two chromophores (Scheme 1b). The benzamides **1a** and **1b** differ in the bp-substitution pattern, and the alkylamides **1c** and **1d** differ in the stereochemistry of the Tyr  $\alpha$ -carbon atom. The structures of the dyads and of the primary amides **2a–c** that were synthesized as reference compounds are summarized in Scheme 2. Theoretical data on the ground-



Scheme 2. Structures of the dyads **1a–d** and the monochromophores **2a–c**.

state conformations of **1a–d** from molecular-dynamics simulations (Langevin dynamics) were used to trace the effects of steric constraints on the probability of head-to-tail interactions between the remote groups in the ground state. Extended NMR-spectroscopic studies yielded information about the distribution of Tyr side-chain rotamers, the solvation of the phenol and the amide functions, the possibility of NOE contacts, and intramolecular aromatic–aromatic interactions.

The probabilities of head-to-tail contacts are compared with the effects of the dyad structures on the rate constants and selectivity of the intramolecular H-atom-transfer reaction in the triplet-excited state. Mechanistic features of the overall UV-light-induced reactions, that is, transient lifetimes, were studied by nanosecond laser flash photolysis (LFP). The determination of quantum yields of the primary reactions is based on spectral resolution techniques. Inter-molecular and intramolecular quenching rate constants were obtained by LFP and the efficiencies of irreversible reaction pathways were tested by steady-state UV-light photolysis. In addition, medium effects were studied in a selection of solvents of similar viscosity, but of different polarity: dichloromethane ( $\text{CH}_2\text{Cl}_2$ , nonpolar), acetonitrile ( $\text{CH}_3\text{CN}$ , polar nonprotic), and methanol ( $\text{MeOH}$ , protic).

## Results and Discussion

### Ground-state structures and conformations

#### $^1\text{H}$ NMR studies

**a) Amide proton resonances:** The chemical shifts of the amide-proton resonances,  $\delta(\text{NH})$ , their temperature coefficients,  $d\delta(\text{NH})/dT$ , and the constants for vicinal coupling with the  $\alpha$  protons,  $^3J(\text{H}^\alpha\text{NH})$ , were used to trace the conformations of the peptide backbone and the presence of electronic effects.  $^1\text{H}$  NMR spectra of the dyads **1a–d** in  $\text{CDCl}_3$  reveal significant differences in the amide-resonance pattern, which can be related to the respective chemical nature of the benzamide (**1a,b**) and alkylamide (**1c,d**) linkers of the dyads. Similar differences are observed for the monochromophoric amides **2a–c**. The chemical shifts,  $\delta(\text{NH})$ , range from 5.9 ppm for the alkylamides **1c,d** and **2c** to 6.9 ppm for the benzamides **1a,b** and **2a,b** in  $\text{CDCl}_3$ . The strong downfield shifts in **1a,b** and **2a,b** by 1 ppm reflect the electronic-withdrawing effect of the  $\pi$  system of benzophenone on the amide group due to conjugation of the amide group with the bp-aromatic system. Notably, this withdrawing effect is transferred also through the Tyr side chain of the benzamides **1a** and **1b**. With respect to **1c,d**, the  $\text{H}^\alpha$  and  $\text{H}^\beta$  resonances of **1a,b** are downfield shifted by +0.4 and +0.2 ppm, respectively (see Figure 1a for labeling of the hydrogens).

The temperature coefficient of the amide-proton resonance,  $d\delta(\text{NH})/dT$ , is a valuable tool for tracing the hydrogen-bonding (HB) situation of peptides in solution. Intramolecular HB of the amide group cannot be expected to be significant for the structures in this study. However, intermolecular HB due to aggregation might well be a significant mechanism for the concentrations used in NMR ( $\approx 25$  mM). Values of  $-7.1$  and  $-7.6$  ppb  $\text{K}^{-1}$  were obtained for **1c** and **1d**, respectively, in  $\text{CDCl}_3$  solutions in the temperature range  $223 < T < 313$  K. These strong upfield shifts of the amide resonances as temperature increases are in accord with free amide protons that are not involved in hydrogen

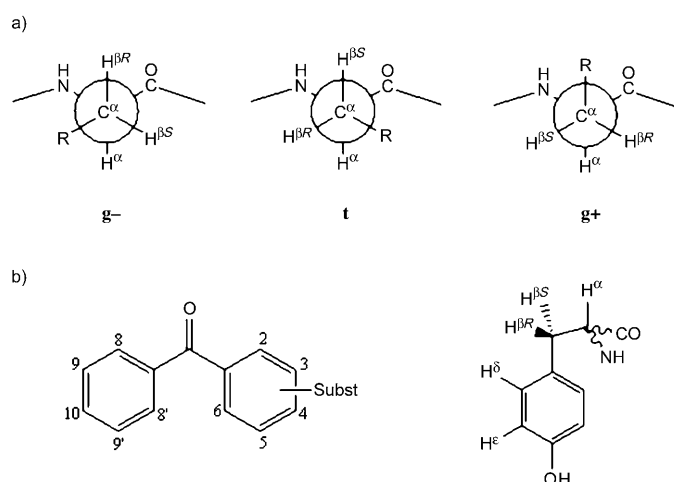


Figure 1. a) Newman projections of the (*S*)-Tyr side chain along the  $\text{C}^\alpha\text{--C}^\beta$  bond with  $\text{R}=4\text{-phenol}$ ; the three possible staggered rotamers are assigned as the two *gauche*- ( $g^-$  with  $\chi^1 = -60^\circ$  and  $g^+$  with  $\chi^1 = +60^\circ$ ) and one antiperiplanar ( $t$  with  $\chi^1 = -180^\circ$ ) conformations with respect to the relative orientation of the highest priority substituents  $\text{-NH-}$  and  $\text{R}$ , respectively. b) Assignment of hydrogen atoms in the bp (3/4-substitution) and Tyr moieties of bpUTyr dyads.

bonding, and are taken as a strong argument against aggregation. The same argument should hold for the much lower concentrations of the dyads employed in the photochemical part of the study ( $< 2$  and  $< 0.1$  mM at 355 and 266 nm, respectively).

The amide resonances of **1a–d** are split into well-resolved doublets in all cases by coupling with the protons on the  $\alpha$ -carbon atom of Tyr. The underlying vicinal coupling constants,  $^3J(\text{H}^\alpha\text{NH})$ , can be associated with the torsion about the  $\text{N(H)–C}^\alpha$  bond in the peptide backbone. These coupling constants are widely used to infer the secondary structure of peptides in solution.<sup>[10]</sup> It was reported that most linear peptides give rise to coupling constants higher than 7.0 Hz. These values are not far from the coupling constants of 8.5 Hz in  $\beta$  sheets, which represent the prototype of “backbone-extended structures”. Note that the terms “extended structure” and “folded structure” will be used below in the discussion to describe the distance between the aromatic moieties in the dyads, which do not necessarily refer to the torsion of the backbone. In our case the dyads consistently yielded values of  $7.8 \pm 0.1$  Hz for the vicinal coupling constants. No influence of the medium on the coupling constants was observed during experiments in eight nonprotic deuterated solvents. A dominance of backbone-extended structures can be concluded for all of the dyads **1a–d** in all media under investigation. In contrast, the chemical shifts of the amide resonances are strongly dependent on the properties of the solvent. Downfield shifts of  $> 2.0$  ppm were observed in solvents such as DMSO, THF, and DMF, and these are ascribable to H-bonding of the amide NH group to the solvent.

**b) Side-chain rotamer populations:** The molecular structure of the dyads can be clarified further through a study of their

$^1\text{H}$  NMR coupling constants. In particular, the vicinal coupling constants between the diastereotopic  $\beta$  protons and the  $\alpha$  proton of the Tyr side chain,  $^3J(\text{H}^\alpha, \text{H}^{\beta\text{R}})$  and  $^3J(\text{H}^\alpha, \text{H}^{\beta\text{S}})$ , are key in probing the rotamer populations of the Tyr side chain (Figure 1a). With a view to the anticipated solvent dependence of the photochemical reactivity, the spin systems were analyzed in a number of deuterated solvents. Based on the Karplus equation,<sup>[11]</sup> which correlates a coupling constant with a dihedral angle, the vicinal coupling constants,  $^3J(\text{H}^\alpha, \text{H}^{\beta\text{R}})$  and  $^3J(\text{H}^\alpha, \text{H}^{\beta\text{S}})$ , were used to derive fractional populations  $p_{\text{g}-}$ ,  $p_{\text{t}}$ ,  $p_{\text{g}+}$  of rotamers in the tyrosine side chain by using Equations (1–3) (see Figure 1b for labeling of the Tyr protons).<sup>[12,13]</sup> The notation of the rotamers is based on the dihedral angle  $\chi^1$  between the  $\text{N}-\text{C}^\alpha-\text{C}^\beta$  plane and the  $\text{C}^\alpha-\text{C}^\beta-\text{C}^\gamma$  plane of the Tyr side chain (the superscripts  $n$  of the dihedral angles  $\chi^n$  define the position in the amino acid side chain). Conformations  $\text{g}-$ ,  $\text{t}$ , and  $\text{g}+$  correspond to  $\chi^1 = -60^\circ$ ,  $-180^\circ$ , and  $+60^\circ$ , respectively. Note that the **1d** configuration at  $\text{C}^\alpha$  is reversed, that is, the assignment of the rotamers  $\text{g}+$  and  $\text{g}-$  is reversed to  $\chi^1 = -60^\circ$  and  $+60^\circ$ , respectively. The geminal protons  $\text{H}^{\beta\text{R}}$  and  $\text{H}^{\beta\text{S}}$  (Figure 1a) were assigned as the high-field and the low-field, respectively, part of the AB subspectrum at 3.0 ppm.<sup>[14]</sup>

$$p_{\text{g}-} = [^3J(\text{H}^\alpha, \text{H}^{\beta\text{R}}) - ^3J_{\text{g}}] / \Delta^3J \quad (1)$$

$$p_{\text{t}} = [^3J(\text{H}^\alpha, \text{H}^{\beta\text{S}}) - ^3J_{\text{t}}] / \Delta^3J \quad (2)$$

$$p_{\text{g}+} = 1 - p_{\text{g}-} - p_{\text{t}} \quad (3)$$

In Equations (1–3),  $\Delta^3J = ^3J_{\text{t}} - ^3J_{\text{g}}$ , in which  $^3J_{\text{t}}$  and  $^3J_{\text{g}}$  are the nominal values of the coupling constants for the vicinal protons in the *trans* and *gauche* conformations, respectively. Values of  $^3J_{\text{t}} = 13.56$  Hz and  $^3J_{\text{g}} = 2.60$  Hz were used in the calculations.<sup>[15]</sup> Experimental coupling constants were derived by simulation of the ABX spin systems with the MestReC program. With an error in  $^3J(\text{H}^\alpha, \text{H}^{\beta(\text{S/R})})$  of  $\pm 0.2$  Hz, the resulting errors in rotamer populations are estimated to be  $\pm 0.03$  and  $\pm 0.05$  for  $p_{\text{g}-}$  ( $p_{\text{t}}$ ) and  $p_{\text{g}+}$ , respectively. The measured coupling constants for **1a–d** and the computed fractional distributions for rotamers  $\text{g}-$ ,  $\text{g}+$ , and  $\text{t}$  are summarized in the Supporting Information, Tables S1 and S2. Note that the intrinsic uncertainty of the population of  $\text{g}+$  is large for small absolute values of  $p_{\text{g}+}$ . It has recently been found that the chosen formalism of population derivation tends to overestimate the population of  $\text{g}+$  systematically at low  $p_{\text{g}+}$ .<sup>[16]</sup>

All four bichromophores **1a–d** in  $\text{CDCl}_3$  gave values for  $^3J(\text{H}^\alpha, \text{H}^{\beta\text{R}})$  and  $^3J(\text{H}^\alpha, \text{H}^{\beta\text{S}})$  of around 6.2 and 5.6 Hz, respectively (see Table S1). This invariance suggests that the chemical environments of the  $\text{H}^{\beta\text{R}}$  and  $\text{H}^{\beta\text{S}}$  protons in **1a–d** are closely related. Accordingly, only small differences between chemical shifts of  $\text{H}^{\beta\text{R}}$  and  $\text{H}^{\beta\text{S}}$  [ $\Delta\delta(\text{H}^{\beta\text{R}} - \text{H}^{\beta\text{S}}) \approx 0.06$ – $0.09$  ppm] are observed. This similarity of structures is further corroborated by an analysis of the rotamer distributions. Thus, in  $\text{CDCl}_3$  (solvent 2 in Figure 2;  $\epsilon_{\text{solv}} = 4.81$ ),<sup>[17]</sup> there appears to be no expressed preferential conformation

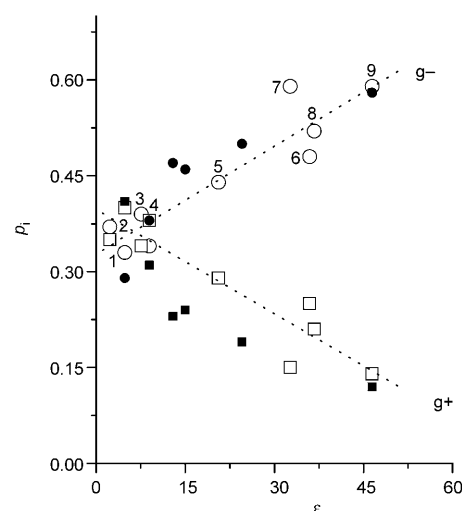


Figure 2. Solvent dependence of the averaged rotamer populations,  $p_i$ , of **1c,d** ( $\text{g}-$ :  $\circ$ ,  $\text{g}+$ :  $\square$ ); filled symbols: data from ref. [18b] for Ac-Tyr-OEt; dotted lines: linear trends; code: 1, [D<sub>8</sub>]dioxane; 2, CDCl<sub>3</sub>; 3, [D<sub>8</sub>]THF; 4, CD<sub>2</sub>Cl<sub>2</sub>; 5, [D<sub>6</sub>]acetone; 6, [D<sub>3</sub>]CH<sub>3</sub>CN; 7, [D<sub>4</sub>]MeOH; 8, [D<sub>7</sub>]DMF; 9, [D<sub>6</sub>]DMSO.

for all compounds in this study. In  $\text{CDCl}_3$  the computed distributions are, within the error limits, not far from a simple uniform statistical weighting with the factor of about one third for all compounds, although there appears to be a slight overrepresentation of the rotamer  $\text{g}+$ . Similar rotamer populations are obtained in  $\text{CD}_2\text{Cl}_2$  solutions (solvent 4 in Figure 2;  $\epsilon_{\text{solv}} = 8.93$ ).<sup>[17]</sup> In contrast, the same computation procedure leads to a substantial loss in the statistical weight for  $\text{g}+$  and a concomitantly significant increase in the statistical weight of  $\text{g}-$  if solvents of higher “polarity”, such as  $\text{CH}_3\text{CN}$  (solvent 6 in Figure 2;  $\epsilon_{\text{solv}} = 35.94$ )<sup>[17]</sup> and  $\text{MeOH}$  (solvent 7 in Figure 2;  $\epsilon_{\text{solv}} = 32.66$ ),<sup>[17]</sup> are considered.

The  $\text{g}-$  selectivity of aromatic amino acid side chains at high solvent polarity is a general phenomenon irrespective of the nature of the aromatic group.<sup>[18–20]</sup> It has been associated with steric effects, however, a satisfying rationalization for this is lacking. As can be seen in Figure 2, the computed rotamer populations  $p_i$  of the alkylamides **1c,d** (given as mean values with an error  $\Delta p_i < 0.02$ ), follow a linear ( $R > 0.92$ ) dependence on the solvent permittivity. A similar dependence ( $R > 0.98$ ) holds for the benzamides **1a,b** (some deviation between the two sets is noted at low permittivity; data not shown). In particular, the populations are correlated with a bulk property of the solvent. Our data are qualitatively in accord with data reported for tyrosine derivatives in several solvents and solvent mixtures (filled symbols in Figure 2).<sup>[18b]</sup> However, in the cited work the rotamer populations of *N*-Ac-Tyr-OEt depended linearly on the decadic logarithm of the permittivity,  $\log \epsilon_{\text{solv}}$ . Because this study was partly based on solvent mixtures, the discrepancy between the data sets might be due to effects of preferential solvation in solvent mixtures. Irrespective of this, all compounds (also those from ref. [18b]) give very similar values of  $p_i$

that are not solvent dependent (data not shown). Essentially, the summed population of the conformers  $g^+$  and  $g^-$ , which are capable of nominally short distances, that is, which fulfil one requisite of reactive contacts between the aromatic moieties ( $t$ , in contrast, does not, see Figure 1a) is independent of the solvent.

*c) Chemical shifts of aromatic protons:* Steric conditions that are favourable for  $\pi$ - $\pi$  interactions between the remote aromatic moieties in the ground state might be reasonably taken to be consonant with favourable conditions for electronic overlap of the reacting partners also in the excited state. Thus, the  $^1\text{H}$  NMR pattern of the aromatic protons of **1a-d** in  $\text{CDCl}_3$  was used to trace the effects of the substitution geometry on the possibility and extent of intramolecular interactions. Both distinct subsections of the region of aromatic protons at 7.3–8.2 ppm (bp) and 6.5–7.0 ppm (Tyr) exhibit evidence for such interactions.

One singlet signal assigned as the  $\text{H}^2$  resonance of bp (see Figure 1b for numbering of the protons in the bp rings) is affected selectively in the presence of Tyr. A subtle high-field shift from 7.77 for **2c** to 7.68 for **1c** and 7.64 ppm for **1d** is observed. The remaining bp subspectra of **1c** and **1d** are convincingly reproduced by the model compound **2c**. Selective shielding of the  $\text{H}^2$  proton is also observed for the benzamide **1a**. However, the introduction of a second carbonyl substituent to the *meta* position of the benzamides **1a** and **2a** significantly affects also the resonances for  $\text{H}^4$ ,  $\text{H}^5$ , and  $\text{H}^6$  of bp (see Figure 1b for numbering of the bp rings). Two contrary effects can be separated: 1) Chemical shifts associated with the resonances of  $\text{H}^2$ ,  $\text{H}^4$ , and  $\text{H}^6$  for **2a** are significantly shifted to lower field by  $+0.2 < \Delta\delta < +0.4$  ppm with respect to the alkyl-amide substituted **2c**. This shift is attributed to the additional withdrawing effect of the second carbonyl group. On the other hand, 2) the presence of the Tyr residue in **1a** causes a high-field shift of the resonance of  $\text{H}^2$  by  $-0.15$  ppm with respect to the monochromophore **2a**. For the *para*-substituted **1b** and **2b** no significant differences between the bp subspectra are observed.

The characteristic “pair of doublets” pattern of the AA'BB' spin system of the Tyr moiety in  $\text{CDCl}_3$  yields valid additional evidence for the interactions within the bp/Tyr dyads (Figure 3). The assignment of  $\text{H}^b$  and  $\text{H}^e$  (see Figure 1b for labeling of the Tyr protons) as the low-field and high-field pseudo-doublets, respectively, was based on NOE experiments. The observed effects are limited to the keto-profen-based dyads **1c,d**; 1) selective shielding of aromatic Tyr proton resonances and 2) decreasing chemical-shift differences between the  $\text{H}^b$  and  $\text{H}^e$  resonances of Tyr. The dyads **1c,d** experience a significant high-field shift of their  $\text{H}^b$  and  $\text{H}^e$  resonances with respect to **1a,b** and free Tyr, for which values of  $\delta(\text{H}^b) = 7.16$  ppm and  $\delta(\text{H}^e) = 6.85$  ppm have been reported.<sup>[21]</sup> For **1c,d** the *meta* protons  $\text{H}^b$  are significantly shielded by  $-0.15$  and  $-0.35$  ppm, respectively, relative to the respective chemical shifts in **1b**. Weaker shielding is observed for the *ortho* protons  $\text{H}^e$  with  $-0.03$  and

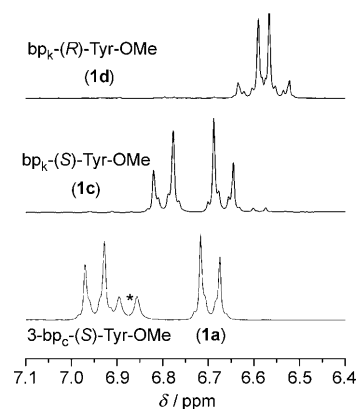


Figure 3. Region of Tyr aromatic proton resonances of the  $^1\text{H}$  NMR spectra (200 MHz,  $\text{CDCl}_3$ ) of **1d** (upper trace), **1c** (middle trace), and **1a** (lower trace); asterisk: amide-proton resonance.

$-0.15$  ppm for **1c** and **1d**, respectively, relative to the respective chemical shifts in **1b**.

Similarly affected Tyr subspectra were reported for other Tyr/ketone dyads in  $\text{CDCl}_3$ , but no explanation was given.<sup>[6a]</sup> A rationalization of the upfield shifts could invoke intramolecular H-bonding between the bp and the Tyr moieties in weakly HB-accepting solvents such as  $\text{CDCl}_3$ . However, the observed chemical shifts of the resonances at 6.1 and 6.0 ppm for the acidic phenol protons of **1c** and **1d** in  $\text{CDCl}_3$  rule out any significant contribution from intramolecular H-bonding. H-bonding usually gives rise to strong low-field shifts of the phenol proton resonance to  $\delta > 10$  ppm.<sup>[22]</sup> Strong downfield shifts of the resonances of the phenol hydroxyl group were actually observed in HB-accepting solvents. These solvent-dependent shifts are fully in accord with the linear dependence of the hydroxyl chemical shifts on the HB-acceptor ability of the solvent.<sup>[23]</sup> In addition, analogues of **1c,d** in which the phenolic functions are protected as methoxy groups show NMR spectra in  $\text{CDCl}_3$  that are very similar to the spectra of their parent compounds.<sup>[24]</sup>

However, it is well known that aromatic amino acids are susceptible to aromatic–aromatic (A–A) interactions.<sup>[25]</sup> Illustrative cases of strong A–A interactions have been reported for neighboring aromatic residues in a cyclic dipeptide and across the strands of a  $\beta$ -hairpin mimic. Here, the proton  $\text{H}^b$  of Tyr is located inside the anisotropic cone of another aromatic side chain connected to a high-field shift of the resonance frequency even beyond the one of  $\text{H}^e$ .<sup>[26]</sup> It is suggested that the observed shielding of  $\text{H}^2$ ,  $\text{H}^b$ , and  $\text{H}^e$  in **1c,d** also reflects a “ring-current” effect due to close contacts between the aromatic moieties of **1c,d** (see Figure 3). The interpretation is corroborated by the results of NOE experiments (see below) and by the solvent dependence of the NMR pattern of the aromatic Tyr protons.

*d) Aromatic–aromatic interactions—Medium und steric effects:* Interactions between the aromatic moieties were probed in a study of the aromatic-proton resonance pattern in the NMR spectra of **1a-d** in several deuterated solvents.

Two parameters were chosen to analyze the effects on the chemical shifts of the aromatic protons: 1) The spectral width of the Tyr AA'BB' spin system of each dyad,  $|\Delta\delta(\text{H}^\delta - \text{H}^\epsilon)| = |\delta(\text{H}^\delta) - \delta(\text{H}^\epsilon)|$ , and 2) ring-current effects (*rce*) that focus on single aromatic protons ( $\text{H}^\delta$  or  $\text{H}^\epsilon$ ) and are defined as the difference between the chemical shift of one of these protons in a reference compound (i.e., without A–A interactions) and the chemical shift of an analogous proton in a dyad under study:  $\Delta\delta(\text{dyad}-\mathbf{1b}) = \delta(\text{dyad}) - \delta(\mathbf{1b}) = rce$ .<sup>[27]</sup> Because steric constraints do not allow significant overlap of the aromatic moieties in **1b** (see below), this dyad was chosen as a reference compound.

As mentioned above, the Tyr AA'BB' spectral widths obtained for the alkylamides **1c,d** in  $\text{CDCl}_3$  are substantially smaller than the ones of the benzamides **1a,b**. Interestingly, this general order of spectral widths ( $\mathbf{1a} \approx \mathbf{1b} \gg \mathbf{1c} > \mathbf{1d}$ ) is conserved throughout a survey of nine solvents with greatly varying properties. The spectral widths (Figure 4) correlate to the parameter  $\beta_2^{\text{H}}$  that characterizes the solvent's ability to act as an acceptor for H-bonding. This quantity with values from 0.00 for non-HB-accepting solvents to 1.00 for strongly HB-accepting solvents was defined by Abraham and co-workers in order to construct a Gibbs-energy-related HB-basicity scale.<sup>[28]</sup> As was suggested recently,<sup>[7f]</sup> a corrected value of  $\beta_2^{\text{H}} = 0.15$  for  $\text{CH}_2\text{Cl}_2$  is used in our study.

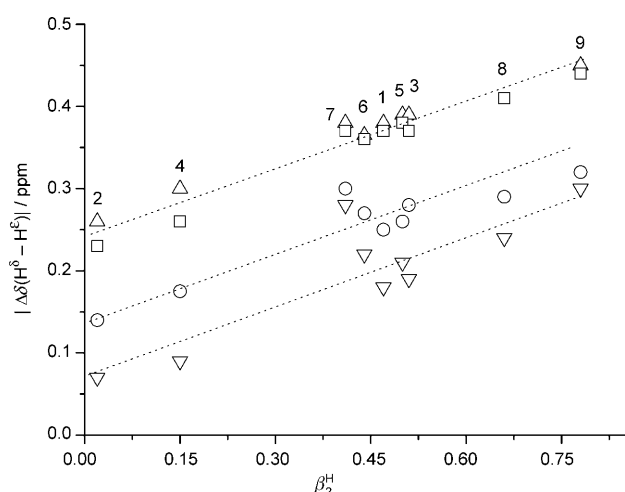


Figure 4. Solvent dependence of  $^1\text{H}$  NMR spectral widths of the AA'BB' spin system of **1a** ( $\Delta$ ), **1b** ( $\square$ ), **1c** ( $\circ$ ), and **1d** ( $\nabla$ ); number code as in Figure 2; the experimental uncertainty of the spectral widths is estimated to be  $\pm 0.02$  ppm.

The spectral widths of the Tyr resonances of **1a–d** obey linear dependencies on the solvents' HB-acceptor abilities. Significant deviations from linearity are solely observed in MeOH solutions (number 7 in Figure 4;  $\beta_2^{\text{H}} = 0.41$ ) as the only protic solvent under study. Interestingly, the dyads **1a–d** yield common slopes but dyad-specific intercepts. The structure-independent slopes as  $\beta_2^{\text{H}}$  increases (slope  $\approx 260$  ppb) can be explained by specific interactions of the phenol hydroxyls with the solvents. Direct evidence for H-

bonding between the phenol and the solvent is taken from the medium effect on the chemical shift of the phenolic-proton resonance. A substantial deshielding of this resonance by  $>3.0$  ppm is observed in highly HB-accepting solvents like DMSO and THF. The H-bonding increases the electron density on the phenolic oxygen<sup>[2h]</sup> and, consequently, the electron density on the *ortho* and *para* carbon atoms of the phenol. This electronic effect can be read from the shielding of the *ortho* protons ( $\text{H}^\epsilon$ ) (e.g.,  $\Delta\delta(\text{H}^\epsilon) = -0.11$  ppm for **1b**) upon going from  $\text{CDCl}_3$  to  $[\text{D}_6]\text{DMSO}$ . The concomitant deshielding of  $\text{H}^\delta$  by 0.10 ppm indicates a decreased electron density at the *meta* carbon atoms.

The contributions of the solvents and the dyads' structures to the observed spectral widths can be separated. We suggest that the dyad-structure-controlled A–A interactions manifest themselves in the variation of the intercepts in Figure 4. This conclusion is further corroborated if ring-current effects, *rce*, on the chemical shifts of  $\text{H}^\delta$  and  $\text{H}^\epsilon$ , as defined above, are considered (Figure 5). In fact, the obtained *rce* values depend only weakly on the solvent (slope  $\approx 70 \pm 10$  ppb), indicating similar probabilities for head-to-tail interactions in all solvents. This is in accord with the previously discussed invariance of the summed population of the rotamers *g+* and *g-* (see discussion of Figure 2).

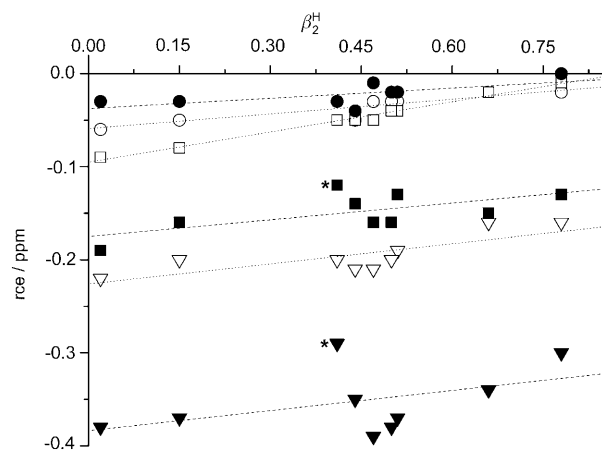


Figure 5. Solvent dependence of the ring-current effects, *rce* (see text), of **1a** (circles), **1c** (squares), and **1d** (triangles); full and open symbols denote the aromatic Tyr protons  $\text{H}^\delta$  and  $\text{H}^\epsilon$ , respectively; asterisk: data in  $[\text{D}_4]\text{MeOH}$ ; lines correspond to linear fits to the experimental data; experimental uncertainty of the *rce* is estimated to be  $\pm 0.02$  ppm.

Structure-dependent variation in the absolute values of the *rce* dominates the plots. The alkylamides **1c,d** generally show higher *rce* values than the benzamides **1a,b**. In addition, the A–A interactions induce site-specific ring-current effects in **1c,d**. The *meta* protons  $\text{H}^\delta$  of Tyr appear to be closer to the anisotropic cone(s) of one or both of the biphenyl moieties than the *ortho* protons  $\text{H}^\epsilon$ . This conclusion was further addressed by NOE experiments (see below). Importantly, the ring-current effects are significantly different for the epimeric dyads **1c** and **1d**. Thus, the probability of head-to-tail contacts between the aromatic moieties, that is,

the electronic overlap of the chromophores, is affected by the regiochemistry (as in **1a** and **1b**) and the stereochemistry of the chromophores.

*e) NOE spectroscopy—Intramolecular folding:* Nuclear Overhauser enhancement spectroscopy, NOESY, supplements the information available from usual NMR experiments. In addition to scalar-coupling phenomena, NOESY yields information on the coupling of nuclear spins through space. NOESY is performed by saturating the NMR frequency of a selected nuclear spin and measuring the enhancements,  $I_{\text{NOE}}$ , in the intensities at the resonance frequencies of neighboring nuclear spins. The key feature of NOESY of interest to this investigation is that the measured  $I_{\text{NOE}}$  are a function ( $I_{\text{NOE}} \propto r^{-6}$ ) of the distances,  $r$ , between the saturated nuclear spin and its respective neighbors.

1D-NOESY experiments in  $\text{CDCl}_3$  were undertaken for **1a** and **1c,d** in order to address the structural peculiarities of the interaction between the aromatic moieties. Similar NOE patterns were obtained for both alkylamide dyads **1c,d**. Because the above  $^1\text{H}$  NMR spectra showed aromatic interactions and, hence, indicated folding of the dyads, NOE signals that are indicative of short contacts between the aromatic Tyr and other parts of the molecule are of special interest.

A strong NOE is observed for the interaction of Tyr  $\text{H}^\delta$  with the amide proton. This is in accord with the computed rotamer populations of **1c** and **1d** in  $\text{CDCl}_3$  (see Table S2 and Figure 2), which exhibited a statistical weight of approximately 70% for the conformations ( $p_{\text{g-}} + p_{\text{g+}}$ ) that allow for small distances between NH and the phenol part of Tyr (Figure 1a).

The amide itself strongly interacts with the  $\text{H}^2$  of bp. This finding outlines substantial folding of the dyads **1c,d**. The position that would normally be suspect in any folding of the moieties is the chiral aliphatic linkage between bp and Tyr. Apparently, folding of the molecule produces structures in which the protons of the keto-profen-based alkyl group and the Tyr phenol point in opposite directions. This is suggested because, apart from trivial contacts, NOE contacts of these protons are limited to the amide proton.

Instructive NOE signals are obtained upon saturation of the Tyr  $\text{H}^\delta$  resonances ( $\delta(\text{H}^\delta) = 6.80$  and  $7.0$  ppm in  $\text{CDCl}_3$  and  $\text{CH}_3\text{CN}$ , respectively; negative signals in Figure 6). In  $\text{CDCl}_3$  solutions, contacts of the Tyr  $\text{H}^\delta$  with H atoms on both benzophenone rings are evident (Figure 6a'). The Tyr  $\text{H}^\delta$  protons clearly interact with the  $\text{H}^2/\text{H}^4$  and  $\text{H}^8/\text{H}^6$  protons of the bp moiety. These interactions of the Tyr phenol ring with the remote bp phenyl rings are suggested to be the source of the observed high-field shift of the  $\text{H}^\delta$  resonance of **1c,d** in  $\text{CDCl}_3$  (Figure 3). As previously discussed, the ring-current effects in **1c,d** (Figure 5) are expressed more for the  $\text{H}^\delta$  protons than for the  $\text{H}^\epsilon$  protons. This site-selectivity of ring-current effects could be interpreted as a consequence of the  $\text{H}^\delta$  protons being at a closer distance to the bp-ring system than the  $\text{H}^\epsilon$  protons.

Very similar NOE intensities are observed after saturation of the  $\text{H}^\epsilon$  resonances of **1c,d**. This finding points to a similar distance distribution in both compounds. Thus, ring-current effects and NOE intensities that describe the geometry of remote aromatic moieties have to be taken as complementary parameters.

This conclusion is in accord with the observed NOEs of benzamide **1a**, that exhibits moderate and strong NOEs with  $\text{H}^2/\text{H}^4$  on saturation of the  $\text{H}^\delta$  and  $\text{H}^\epsilon$  resonances, respectively. The strong NOEs are contrasted by negligible

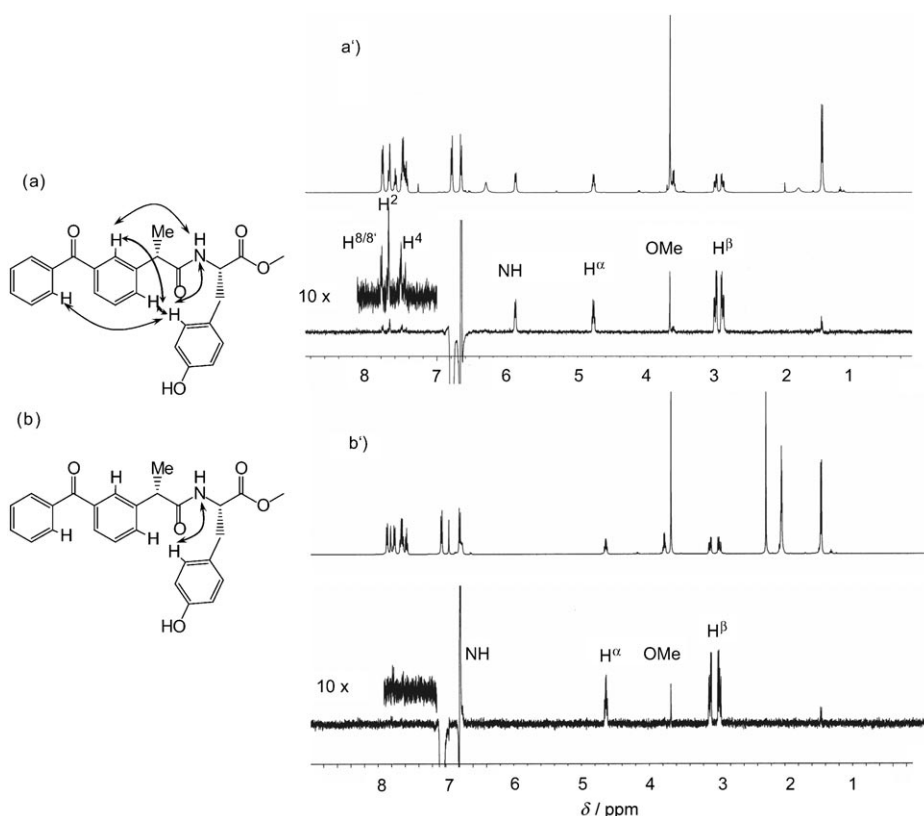


Figure 6. Left column: Schematic views of selected NOE contacts obtained for **1c** in a) chloroform and b) acetonitrile. Right column: Comparison of 500 MHz  $^1\text{H}$  NMR (upper traces) obtained for **1c** in a') chloroform and b') acetonitrile and respective NOE spectra (lower traces) obtained after saturation of the  $\text{H}^\delta$  resonance of **1c**.



ring-current effects (Figure 5). Due to the short linker between the chromophores in **1a**, close contacts between the aromatic systems are inevitable. Thus, the close contacts between the aromatic moieties as in **1a** are not necessarily associated with effective geometric overlap of the  $\pi$  systems.

Additional NOE experiments on **1c** in  $\text{CD}_3\text{CN}$  solution (Figure 6b') show that the probability of close contacts between the remote aromatic moieties is greatly reduced in this solvent of higher HB-acceptor ability. In particular, there is no significant NOE between the Tyr  $\text{H}^\delta$  and the bp  $\text{H}^2$ . In addition, the NOE between the amide proton and the  $\text{H}^2$  that was prominent in  $\text{CDCl}_3$  solution is missing in  $\text{CH}_3\text{CN}$ . However, the selective shielding due to ring-current effects was shown to be only weakly solvent dependent (Figure 5). This necessarily means that the change from chloroform to  $\text{CH}_3\text{CN}$  induces a change in the average structure of **1c** from a condensed (many NOE contacts in chloroform) to a more extended one (few NOE contacts in  $\text{CH}_3\text{CN}$ ), which still allows for interactions between the aromatic moieties.

In contrast, the NOE contacts observed for **1d** remain totally unaffected by this change in the solution medium. It is concluded that the probability of the condensed structures of **1d** is preserved also in solvents of high HB-acceptor ability.

**Langevin dynamics for distance distributions:** The observed close contacts between the two aromatic moieties point to the possibility of conformers with close hydroxyl/carbonyl contacts  $r_{\text{O}\cdots\text{O}}$  also. Intrinsically, NOESY cannot supply quantitative information on the distance between the phenol hydroxyl and the bp carbonyl. However, the latter distance can be investigated with molecular-dynamics simulations (Langevin dynamics) using umbrella sampling for **1a–d**. The starting structures were obtained by steric energy minimizing. Sampling of **1c** and **1d** in a dielectric continuum with the permittivity set to  $\epsilon=37$  as a mimic of acetonitrile solution similarly gave a very narrow pair-distribution function with a maximum at a distance  $r_{\text{O}\cdots\text{O}}=2.7$  Å. Such short distances are usually indicative of strong hydrogen bridges, which were also observed in the solid state,<sup>[6a]</sup> and are seen as DFT ground-state minima for dyads that are structurally closely related<sup>[6d]</sup> to the ones in the current work.

However,  $^1\text{H}$  NMR of the hydroxyl protons at  $\delta < 6$  ppm and  $< 7$  ppm rule out that there are any significant contributions from intramolecular hydrogen bridges at room temperature both in  $\text{CDCl}_3$  and  $\text{CD}_3\text{CN}$ , respectively. Thus, results from molecular dynamics are treated to be unrealistic in the sense that they artificially overestimate the formation of hydrogen bridges.

To overcome the limitations of the methodology, the permittivity of the dielectric continuum was set to infinity to suppress the influence of Coulombic forces. Under these restraints, contributions from hydrogen bonding are effectively inhibited. However, the resulting molecular-dynamics simulation still yields close contacts of hydroxyl and carbonyl occurring with significant probability in **1a** and **1c** (Figure 7).

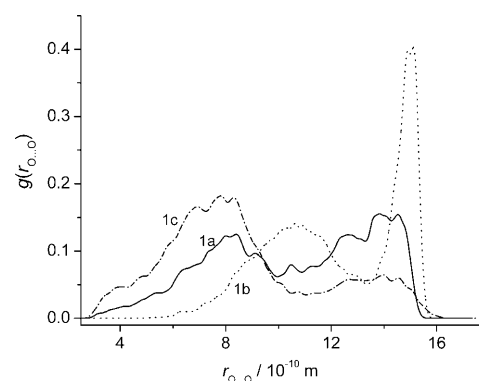


Figure 7. Pair-distribution functions of carbonyl–hydroxylic group distance  $r_{\text{O}\cdots\text{O}}$ , obtained with umbrella sampling according to Equation (14) for **1a** (—), **1b** (.....), and **1c** (---).

The pair-distribution functions in Figure 7 for **1a–c** were obtained after averaging three differential distributions that were computed for three individual starting conformations of the Tyr side chain, corresponding to  $g-$ ,  $t$ , and  $g+$ , respectively. For **1a,b** the resulting three differential pair-distribution functions were very similar to each other. Thus, the method can be safely assumed to sample efficiently the accessible conformational space for these two compounds.

The situation appeared to be different for **1c,d** (**1d** exhibits a distribution similar to **1c** with a tendency to less-favoured close contacts). Here, the individual pair-distribution functions for each molecule differed significantly among themselves, and the average distribution for **1c** should only be used for qualitative conclusions. Umbrella sampling appears not to cover the whole conformational space for these two ketoprofen-based dyads; that is, the conformational freedom of the (*S*)-2-phenylpropionylamide moiety extends the range of possible ground-state minima that have to be accounted for and sampled properly. A current study addresses the dynamics of **1c,d** in further detail. Nevertheless, the main results remain unaffected. The probability of short contacts between the ketone and the phenol is strongly dependent on the molecular structure. The presence of a rigid amide bond in the *para* position of the benzamide **1b** confines the accessible space of the remote groups in a way such that close contacts between the ketone and the phenol are completely inhibited (..... in Figure 7). Moving the amide substituent to the *meta* position partly relieves the steric constraints for close contacts (shown curve in Figure 7). Furthermore, this effect appears to be enhanced by increasing the flexibility of the linkage between the chromophores on going from **1a** to **1c** (--- in Figure 7).

## Excited-state dynamics

**Photophysical and photochemical properties—Steady-state experiments:** The photophysical properties of the dyads were studied to trace possible effects of the substitution geometry on the electronic properties of the bp moiety. The ultraviolet absorption spectra of the compounds **1a–d** are

dominated by the intense absorption bands of the aromatic chromophores (Figure 8). The respective band structure depends on the position of ring substitutions and strongly re-

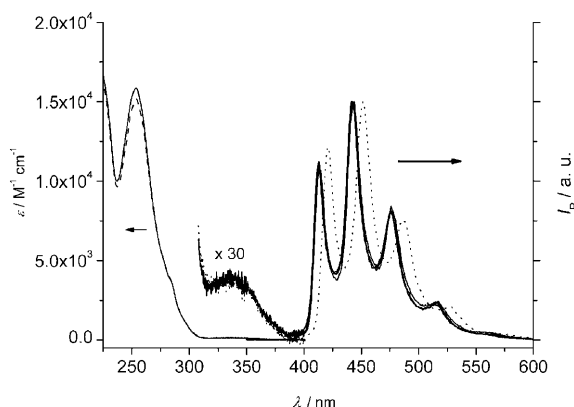


Figure 8. Absorption spectra of **1c** (—) and **1d** (---) and phosphorescence spectra of **1c**, **1d**, **1a**, and bp (continuous lines) and **1b** (dotted line); inset: zoom on the  $n \rightarrow \pi^*$  absorption. Absorption spectra were obtained at 25°C in  $\text{CH}_3\text{CN}$ ; phosphorescence was observed at 77 K in methanol/ethanol (1:1) with concentrations of  $10^{-4}$ – $10^{-3}$  M.

sembles the spectra of the underlying benzophenone parent compounds. The UV-visible spectra of all the compounds are typical for *meta*- and *para*-substituted benzophenones with a maximum absorption at 250 nm (in acetonitrile,  $\epsilon_{\text{bp}}(250 \text{ nm}) = 16000 \text{ M}^{-1} \text{ cm}^{-1}$ ). As usually observed for benzophenones with an  $S_1$  state of  $n \rightarrow \pi^*$  character, the  $S_0 \rightarrow S_1$  transition is only weakly allowed with molar absorption coefficients in the range of  $10^2 \text{ M}^{-1} \text{ cm}^{-1}$ . A shoulder at 280 nm, observed for the dyads **1a–d**, is assigned to the absorption of the Tyr moiety. Both the  $\pi \rightarrow \pi^*$  transition at 255 nm and the weaker  $n \rightarrow \pi^*$  transition at 340 nm (in acetonitrile,  $\epsilon_{\text{bp}}(340 \text{ nm}) \approx 150 \text{ M}^{-1} \text{ cm}^{-1}$ ) exhibit no significant differences between the diastereomers **1c** and **1d** in solvents of different polarity, for example, acetonitrile, methanol, chloroform, benzene, and cyclohexane. A bathochromic shift of the  $\pi \rightarrow \pi^*$  resonances and a hypsochromic shift of the  $n \rightarrow \pi^*$  absorption as solvent polarity increases are in accord with the literature.<sup>[29]</sup>

Phosphorescence emission spectra of **1a–d** were recorded in  $\text{CH}_3\text{CN}$  and methanol/ethanol (1:1) glasses at 77 K with bp as a spectral reference. All of the compounds exhibit the typical emission-band structure of benzophenone (Figure 8 and Table S3). The well-defined vibrational progressions with an energy spacing of approximately  $1700 \text{ cm}^{-1}$  are indicative of the participation of the  $>\text{C}=\text{O}$  functionality in the radiative process. The emission spectra of bp and all of the *meta*-substituted derivatives **1a** and **1c,d** coincide, whereas the spectrum for the *para*-substituted **1b** is significantly red-shifted in both of the media studied. The triplet energies of all of the tested compounds, calculated from the wavelength corresponding to the 0–0 emission in methanol/ethanol (1:1) glasses, fall into a narrow range between 284 and 290  $\text{kJ mol}^{-1}$ . These values are comparable to an  $E_T$  of

289  $\text{kJ mol}^{-1}$  that was found (this work) and reported<sup>[30]</sup> for benzophenone (Table S3). Note that in  $\text{CH}_3\text{CN}$ , the triplet energies are systematically higher by approximately 3–4  $\text{kJ mol}^{-1}$ . The triplet lifetimes of **1a,b** and bp, obtained from phosphorescence decays, are all about 6 ms (77 K). All these emission characteristics are in accord with literature data for bp derivatives.<sup>[30]</sup> We conclude that the electronic structure of the benzophenone unit is not affected by substitution with tyrosine moieties; that is, the lowest-lying triplet states possess  $n \rightarrow \pi^*$  character.

In contrast to the similar photophysical properties of the dyads **1a–d**, the steady-state photochemical behavior showed significant differences between the benzamides **1a,b** and the alkylamides **1c,d**. Steady-state consumption during irradiation of solutions of **1a–d** at 254 or 313 nm in  $\text{CH}_3\text{CN}$ , MeOH, and  $\text{CH}_2\text{Cl}_2$  was quantified by following the disappearance of the characteristic bp  $\pi \rightarrow \pi^*$  absorption at 250 nm by means of UV-visible spectroscopy and HPLC with UV detection. No attempts were made to identify the stable products. Quantum yields of disappearance ( $\Phi_{\text{irr}}$ ) for 313 nm irradiation, based on the oxalate actinometer, are summarized in Table 1. In inert solvents ( $\text{CH}_3\text{CN}$ ,  $\text{CH}_2\text{Cl}_2$ )

Table 1. Summary of steady-state disappearance quantum yields,  $\Phi_{\text{irr}}$ , of **1a–d**.

Compound	$\Phi_{\text{irr}}^{[a]}$		
	$\text{CH}_2\text{Cl}_2$	$\text{CH}_3\text{CN}$	MeOH
<b>1a</b>	0.004	0.038	0.37
<b>1b</b>	0.049	0.036	0.23
<b>1c</b>	0.006	0.001	0.074
<b>1d</b>	0.004	0.001	0.008

[a] Irradiation at 313 nm,  $[\mathbf{1}] \approx 10^{-3} \text{ M}$ ; experimental error  $\pm 10\%$ .

quantum yields for disappearance ( $\Phi_{\text{irr}}$ ) are generally much lower than in MeOH, in which H-atom abstraction from the solvent is an important process. Note that **1c** shows a significantly lower affinity towards solvent H-abstraction than do **1a,b**, whereas **1d** shows low  $\Phi_{\text{irr}}$  in all three solvents. The quantum yields obtained for **1a,b** in  $\text{CH}_3\text{CN}$  depend strongly on concentration. Quantum yields obtained upon irradiation of **1a,b** at 254 nm decrease by a factor more than ten upon lowering the dyad concentration from  $10^{-3}$  to  $10^{-5} \text{ M}$ . Intermolecular processes are concluded to account for the concentration dependence. The same concentration effect was observed for **1b** consumption in  $\text{CH}_2\text{Cl}_2$ . In contrast, **1a** was virtually inert in  $\text{CH}_2\text{Cl}_2$  solution.

**Flash photolysis:** To study how the structural differences of the dyads translate into their photochemical dynamics, time-resolved laser flash photolysis experiments were performed. Excitation of the strong  $\pi \rightarrow \pi^*$  transition ( $\lambda_{\text{max}} = 250 \text{ nm}$ ;  $\epsilon_{\text{bp}}(250 \text{ nm}) = 16000 \text{ M}^{-1} \text{ cm}^{-1}$ ) or the much weaker  $n \rightarrow \pi^*$  transition ( $\lambda_{\text{max}} = 340 \text{ nm}$ ;  $\epsilon_{\text{bp}}(340 \text{ nm}) = 100\text{--}200 \text{ M}^{-1} \text{ cm}^{-1}$ ) of **1–2** in  $\text{CH}_3\text{CN}$  with 266 or 355 nm pulses of a Nd:YAG laser (FWHM 7–9 ns; 5–7 mJ) equally gives rise to strongly absorbing transients with similar absorption patterns immedi-

ately after the flash. Concentrations in the range of  $4\text{--}8 \times 10^{-5}\text{ M}$  and  $2\text{--}3 \times 10^{-3}\text{ M}$  were used at 266 and 355 nm, respectively. The predominance of bimolecular-quenching processes observed for **1a** and **1b** (see below) suggested excitation at 266 nm, with concomitantly lower dyad concentration, in order to study intramolecular processes. For the other compounds (and **1a** in  $\text{CH}_2\text{Cl}_2$ ), excitation at 266 and 355 nm generally gave similar results with respect to reaction-rate constants and spectral shape. However, spectra, obtained with 355-nm photolysis at short delays, experience convolution with solvent Raman scattering in the spectral range of 380–400 nm. In the case of 266-nm photolysis, excitation of both chromophores (bp and Tyr) cannot be avoided. Accordingly, 266-nm excitation produced time profiles at 300–330 nm that exhibited significant but short-lived emission of light from Tyr fluorescence. Based on molar-absorption coefficients measured for separate bp and Tyr moieties, the fraction of light intensity exciting the bp chromophore at 266 nm is estimated to be  $>90\%$ .

a) *Identification of transients and relaxation paths:* The primary transients in all cases can safely be assigned as the triplet states [Eq. (4)] (Figure 9) of the respective benzophenone moieties for the following reasons:

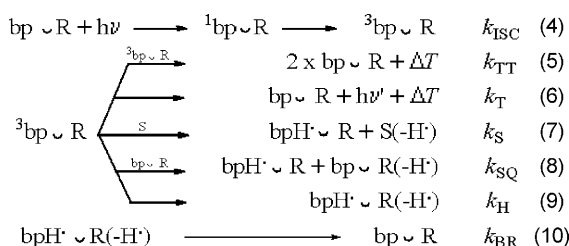


Figure 9. General reaction pattern of the photophysical and photochemical processes of the monochromophoric compounds **2a–c** [Eqs. (4–7)];  $\text{R} = \text{NH}_2$  and dyads **1a–d** [Eqs. (4–10)];  $\text{R} = \text{Tyr}$ ; S denotes a solvent with abstractable hydrogen atoms.

- 1) The small ratios of the observed transient absorbances  $\Delta A$  at 325 and 525 nm (values of 1.6:1) are in accord with reported triplet–triplet (TT) absorption spectra of bp derivatives.<sup>[5b]</sup>
- 2) The molecular absorption coefficients of **1–2** at their respective triplet absorption maxima compare well with a value of  $6500\text{ M}^{-1}\text{ cm}^{-1}$  reported for  ${}^3\text{bp}$  in acetonitrile solution.<sup>[31]</sup> Note that for **1b** and **2b**, that is, *para*-substituted benzophenones, both absorption maxima are red-shifted by 20 nm.
- 3) Long lifetimes of the transients in the microsecond range are observed for all monochromophores and the

bichromophores **1a** and **1b** in acetonitrile. The transient decays for these compounds are not connected with any significant spectral evolutions.

- 4) Transient decays of **1b** and of the monochromophores **2a–c** in inert solvents ( $\text{CH}_3\text{CN}$ ,  $\text{CH}_2\text{Cl}_2$ ) follow mixed kinetics. It is suggested that the second-order component is due to TT annihilation [Eq. (5)]. Clean first-order decays, with lifetimes  $>5\text{ }\mu\text{s}$ , are observed upon a substantial decrease in laser power [Eq. (6)]. Phosphorescence emission from the lowest triplet state was observed for the dyads **1a,b** in  $\text{CH}_3\text{CN}$  solutions.
- 5) The transient absorptions of **1a,b** and **2a–c** are effectively quenched in the presence of molecular oxygen.

All individual decay processes (Figure 9) convolute to give a triplet-decay rate constant,  $k_d$ . At constant light intensity and dyad concentration, the contributions from intrinsic decay ( $k_T$ ), self-quenching ( $k_{\text{SQ}} \times [\text{bpUR}]$ ), and solvent-abstraction reaction ( $k_S \times [\text{S}]$ ) can be summed to give  $k_0$  [Eq. (11)]. Herein, the small contribution from TT annihilation ( $k_{\text{TT}} \times [3\text{bpUR}]^2$ ) is assumed to be negligible at low laser power.

$$k_d = k_T + k_{\text{SQ}}[\text{bpUR}] + k_S[\text{S}] + k_H = k_0 + k_H \quad (11)$$

The general results for the LFP of the dyads are exemplarily discussed for the cases of **1c,d**. For the bichromophores **1c** and **1d** in any solvent, the decay of the initial signals is very rapid, that is, shorter than the triplet decay of monochromophoric **2c** by a factor of  $>100$ . Triplet lifetimes ( $1/k_d$ ) were obtained from mono- or biexponential fits to the transient decays at 600 and 510 nm, respectively. Transient decay is biexponential at 510 nm due to overlap of the absorptions of  ${}^3\text{bp}$  and the ketyl radical,  $\text{bpH}\cdot$  (see below). Triplet lifetimes are between 10 and 60 ns for **1c** and near or below 10 ns for **1d** (see Table 2 for kinetic parameters in  $\text{CH}_2\text{Cl}_2$ ,  $\text{CH}_3\text{CN}$ , and MeOH). The latter values are close to the resolution limit of the laser set-up (because of the laser pulse width) and are thus of qualitative value only. Shorter lifetimes in both cases are observed in dichloromethane solution, whereas the longest triplet lifetimes are observed in MeOH.

Table 2. Solvent dependence of triplet-quenching rate constants  $k_d$ , biradical-formation quantum yields  $\Phi_{\text{BR}}$ , and biradical-decay rate constants  $k_{\text{BR}}$  obtained during the laser flash photolysis of **1a–d** in deoxygenized solvents at 355 nm.

compound	$k_d [10^6 \text{ s}^{-1}]^{[a,b]}$			$k_{\text{BR}} [10^6 \text{ s}^{-1}]^{[c]}$			$\Phi_{\text{BR}}^{[d]}$		
	$\text{CH}_3\text{CN}$	MeOH <sup>[e]</sup>	$\text{CH}_2\text{Cl}_2$	$\text{CH}_3\text{CN}$	MeOH	$\text{CH}_2\text{Cl}_2$	$\text{CH}_3\text{CN}$	MeOH	$\text{CH}_2\text{Cl}_2$
<b>1a</b>	$<0.5^{[f]} (0.30)$	5.9	5.3 (3.2)	— <sup>[g]</sup>	— <sup>[g]</sup>	1.3	$\leq 0.10$	$<0.05$	$>0.9$
<b>1b</b>	$<0.3^{[f]} (0.07)$	5.5	$<1.0^{[f]} (0.80)$	— <sup>[g]</sup>	— <sup>[g]</sup>	— <sup>[g]</sup>	$<0.05$	$<0.05$	$<0.05$
<b>1c</b>	45	37	80	5.6	4.3	12.0	1.0	0.8 <sub>5</sub>	$>0.9$
<b>1d</b>	$\approx 100$	$\approx 100$	$>100$	17.2	11.1	25.0	1.0	0.9 <sub>5</sub>	$>0.9$

[a] From monoexponential fits to transient decays at 470 and 600 nm or biexponential fits at 510 nm with estimated experimental error of  $\pm 5 \times 10^6 \text{ s}^{-1}$  for **1c,d** and  $\pm 0.5 \times 10^6 \text{ s}^{-1}$  for **1a,b**. [b] Values in brackets: intercepts of Stern–Volmer dilution plots. [c] From monoexponential fits to transient decays at 405 nm with estimated experimental error of  $\pm 0.5 \times 10^6 \text{ s}^{-1}$ . [d] Uncertainties are estimated to sum up to  $\pm 0.05$ . [e] In MeOH bimolecular quenching by the solvent<sup>[32]</sup> has to be taken into account [Eq. (7)]. [f] Laser flash photolysis at 266 nm (see text). [g] Not determined due to insignificant formation of biradicals.

The triplet decays of **1c** and **1d** were generally accompanied by spectral shifts from 325 to 335 nm (not shown), 525 to 540 nm, and by growths at 405 nm (Figure 10). This spec-

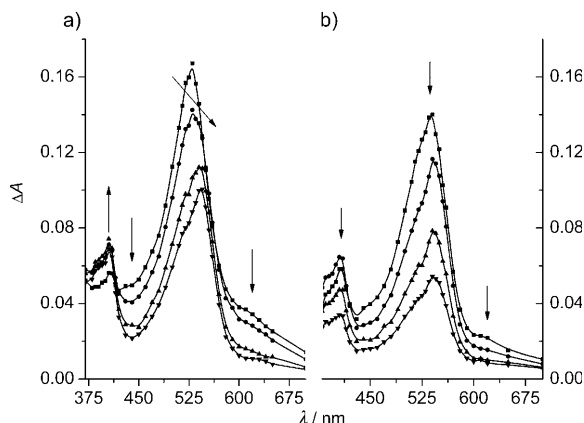


Figure 10. Transient absorption spectra obtained during laser flash photolysis at 355 nm of deoxygenated solutions ( $2 \times 10^{-3}$  M) of a) **1c** and b) **1d** in dry  $\text{CH}_3\text{CN}$ ; time delays after flash (from top to bottom): 17, 27, 50, 75 ns; initial triplet concentration  $[\text{T}]_0 = 55 \pm 5 \mu\text{M}$ .

tral evolution is in accord with fast triplet quenching due to ketyl radical  $\text{bpH}^\bullet$  formation. Concomitant formation of a transient, identified as the tyrosyl radical  $\text{Tyr}(\text{O}^\bullet)$  based on its characteristic double-peak structure at 385 and 405 nm, clearly suggests there is H-atom transfer between a tyrosine moiety and the excited triplet for both diastereomers [Eqs (8,9)]. Furthermore, because the triplet decays of **1c,d** were virtually independent of their dyad concentrations, an intramolecular H-atom-transfer mechanism is surmised for their triplet-state quenching reactions in  $\text{CH}_2\text{Cl}_2$  and  $\text{CH}_3\text{CN}$ . In  $\text{CH}_2\text{Cl}_2$  and  $\text{CH}_3\text{CN}$  transient absorptions decay to zero within, at most, one microsecond for the dyads **1c,d**, whereas the overall transient decays were much slower in MeOH solutions. A residual absorbance at 545 nm, with a lifetime of tens of microseconds, points to the presence of  $\text{bpH}^\bullet$  formed through a different path [Eq. (7)]. A quantitative analysis of the quenching process of **1c,d** in  $\text{CH}_3\text{CN}$  solutions is presented below.

**b) Inter- versus intramolecular H-atom transfer:** The dyads **1a,b** were generally far less reactive than their ketoprofen-based analogues. In contrast to **1c,d**, their triplet lifetimes in  $\text{CH}_3\text{CN}$  and  $\text{CH}_2\text{Cl}_2$  were strongly concentration dependent (Figure 11). Linear Stern–Volmer plots were obtained for both compounds. The observed spectral evolution during triplet decay again is readily interpreted in terms of H-atom transfer. Yields of  $\text{bpH}^\bullet$  and  $\text{Tyr}(\text{O}^\bullet)$  were formed in equal amounts and increased monotonously as dyad concentration increased. Thus, the quenching mechanism is safely assigned as being dominated by self-quenching [Eq. (8)].

The respective self-quenching rate constants  $k_{\text{SQ}}$ , obtained from the slopes of the linear plots for **1a** and **1b**, do not differ significantly from each other (Figure 11). The values

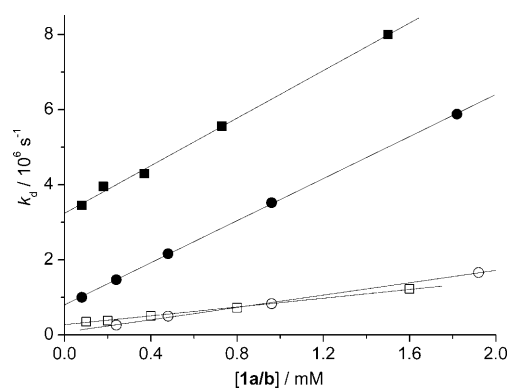


Figure 11. Stern–Volmer plots of triplet-decay rate constants of **1a** (squares) and **1b** (circles) in  $\text{CH}_3\text{CN}$  (open symbols) and  $\text{CH}_2\text{Cl}_2$  (filled symbols); laser photolysis at 355 nm with 7-mJ pulse $^{-1}$ .

for  $k_{\text{SQ}}$  (ca.  $3 \times 10^9 \text{ M}^{-1} \text{ s}^{-1}$  in  $\text{CH}_2\text{Cl}_2$  and ca.  $7 \times 10^8 \text{ M}^{-1} \text{ s}^{-1}$  in  $\text{CH}_3\text{CN}$ ) remain well below the diffusion-controlled limit for both of these solvents. These results are fully in accord with numerous literature data on bimolecular quenching of ketone triplets by phenols, both in regard to absolute values<sup>[4,6b,7e]</sup> and solvent dependencies.<sup>[7a,c,f]</sup> Interestingly, the intercepts of the Stern–Volmer plots for **1a** and **1b** differ greatly in  $\text{CH}_2\text{Cl}_2$ . The triplet-decay rate constants  $k_0$  are not expected to differ markedly for these two dyads because the triplet lifetimes of the monochromophoric compounds **2a** and **2b** were both about 1.5  $\mu\text{s}$  at high dilution in  $\text{CH}_2\text{Cl}_2$ . Thus, in Figure 11, the difference in the intercepts for **1a** and **1b** in  $\text{CH}_2\text{Cl}_2$  has to be looked for in the rate constants for intramolecular quenching,  $k_{\text{H}}$  [Eq. (9)]. In methanol solutions the triplet lifetimes of **1a,b** and **2a–c** were already significantly shortened to  $160 \pm 30$  ns at concentrations in the sub-millimolar range. No attempts were made to study the self-quenching of **1a,b** in MeOH.

The short, intrinsic triplet lifetimes of **1c,d**, due to rapid intramolecular quenching, prevented a direct study of the self-quenching for these compounds. Intermolecular H-atom-transfer rates were addressed instead by quenching of the **2c** triplet with either (*R*)- or (*S*)-configured Boc-Tyr-OMe in  $\text{CH}_3\text{CN}$  (Boc = *tert*-butoxycarbonyl). Stern–Volmer plots for both experiments yielded bimolecular-quenching rate constants of  $2.3 \times 10^8 \text{ M}^{-1} \text{ s}^{-1}$ , which are in reasonable agreement with the measured self-quenching rate constants of **1a,b** (see above). These rate constants are also very close to the results obtained by Miranda et al. for the quenching of a  $\pi \rightarrow \pi^*$  triplet by Boc-Tyr-OMe.<sup>[6e]</sup> The rate constants for the quenching of **2c** with Boc-Tyr-OMe are somewhat smaller than the self-quenching rate constants of **1a,b**. This might be rationalized by the presence of the bulky Boc group, which could potentially hinder a reactive approach. Nevertheless, an important conclusion can be drawn from bimolecular-quenching experiments: irrespective of differing molecular structure and concomitant differences in triplet energies (Table S3), there are no significant differences between the reactivities of **1a–d** toward intermolecular H-atom abstraction from phenols.

To minimize contributions from self-quenching (see above), transient spectra for **1a,b** were also recorded after laser excitation at 266 nm with substantially lower dyad concentrations. Representative spectra recorded for **1a** in different solvents are collected in Figure 12a. In CH<sub>3</sub>CN the triplet state, with its characteristic absorption at 530 nm, is the dominate species 200 ns after excitation (squares in Figure 12a). In MeOH solution the triplet decay is accompanied by formation of a long-lived transient with absorptions at 335 and 545 nm (350 and 575 nm for *para* benzophenones **1b** and **2b**), decaying on a timescale of several tens of microseconds with second-order kinetics. The spectral signature (triangles in Figure 12a) and the observed rate constants allow us to make the assignment of the transient to the ketyl radical bpH<sup>•</sup>. Its formation is rationalized as an abstraction of a hydrogen atom from the solvent [Eq. (7)], and second-order decay is consistent with disproportionation and dimerization. The results for **1b** are very similar to **1a** in methanol and CH<sub>3</sub>CN, respectively. For **1a** in CH<sub>2</sub>Cl<sub>2</sub> solutions 200 ns after the laser flash (circles in Figure 12a), the spectral region around 545 nm strongly resembles the one obtained for **1a** in MeOH. This part of the transient spectrum is presumed to be due to bpH<sup>•</sup> formation. An additional feature at 405 nm is limited to the reaction of **1a** in CH<sub>2</sub>Cl<sub>2</sub>, and is indicative of an efficient formation of Tyr(O<sup>•</sup>). No such transient could be observed for **1b** in CH<sub>2</sub>Cl<sub>2</sub> at comparable concentrations.

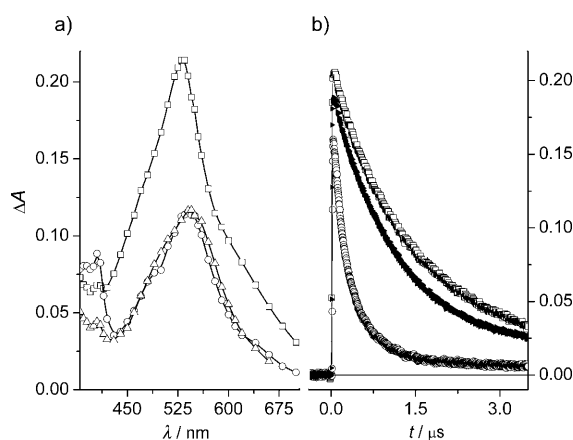


Figure 12. a) Transient spectra obtained 200 ns after 266-nm (5 mJ) laser pulsing of **1a** in CH<sub>3</sub>CN (squares), MeOH (triangles), and CH<sub>2</sub>Cl<sub>2</sub> (circles); b) Transient decay profiles (510 nm) on 266-nm laser pulsing of **1a** in CH<sub>3</sub>CN (squares) and CH<sub>2</sub>Cl<sub>2</sub> (circles), and a profile of **1b** (550 nm) in CH<sub>2</sub>Cl<sub>2</sub> (filled symbols); the latter profile is scaled by a factor of 0.6 for the sake of comparison; concentrations [**1a,b**] =  $8 \times 10^{-5}$  M; initial triplet concentration [T]<sub>0</sub> =  $40 \pm 5$  μM.

c) *Quantitative analysis of intramolecular quenching*: Depending on the molecular structure and the solvent, the lifetimes of the excited triplet decays of **1a–d** range from approximately 10 ns to  $> 5$  μs. The triplet-decay rate constants  $k_d$  obtained from exponential fits to the experimental transient profiles are the sum of rate constants of the individual

decay processes (Figure 9). In inert solvents such as CH<sub>3</sub>CN and CH<sub>2</sub>Cl<sub>2</sub>, the contribution from solvent reactions to the decay constant  $k_0$  in Equation (11) can be neglected. However, in MeOH solutions, the rate constant for triplet-induced H-atom abstraction from the solvent dominates  $k_0$  and must be considered in order to calculate  $k_H$  from the experimentally available  $k_d$  values. The required  $k_0$  values in MeOH solutions were obtained as the rate constant of the triplet decay of the monochromophores **2a–c** in MeOH. These  $k_0$  values ( $(5.5 \pm 0.5) \times 10^6$  s<sup>−1</sup>) do not differ significantly from one another and are in accord with literature data for the triplet decay of bp in MeOH.<sup>[32]</sup>

High selectivity towards H-atom transfer is a common feature of triplet-excited ketone/phenol systems.<sup>[4–7]</sup> However, we are not aware of any reports of quantum yields for the formation of biradicals in ketone/phenol dyads. To address the selectivity of the intramolecular quenching reaction, the transient spectra for **1c,d** in CH<sub>3</sub>CN in this study were deconvoluted into spectral components. Over the complete timescale of the transient decay only the spectral components for <sup>3</sup>bp, bpH<sup>•</sup>, and Tyr(O<sup>•</sup>) are needed to simulate the experimental data quantitatively (Figure 13; upper part). Concentration/time profiles were constructed from spectral resolutions for the reactions of **1c,d** in CH<sub>3</sub>CN (Figure 13; lower part). The rate of formation of the radical species is, within experimental error, identical to the triplet-decay rate of **1c**. For **1d** the triplet decay is already strongly convoluted with the excitation laser profile. These triplet decays are connected with formation of equimolar amounts of bpH<sup>•</sup> and Tyr(O<sup>•</sup>). Formation and decay of both radicals appear to follow the same time law, which is in accord with an intramolecular-reaction mechanism. The formation of biradicaloid intermediates bpH<sup>•</sup>Tyr(O<sup>•</sup>) [Eq. (9)] is analogous to intermediates that were reported for a number of related dyads.<sup>[4,5a–d,6a,c,d]</sup> The biradicals, BR, decay exponentially on a longer timescale [Eq. (10)] than do the triplets with  $k_d \approx 5$ – $10 \times k_{BR}$ . Note that the rate constants for triplet quenching ( $k_d(\mathbf{1d})/k_d(\mathbf{1c}) \approx 2$ ) and BR decay ( $k_{BR}(\mathbf{1d})/k_{BR}(\mathbf{1c}) \approx 2$ – $3$ ) exhibit some diastereoselectivity, irrespective of the solvent. Similar observations have been made with related dyads.<sup>[6a,c,d]</sup>

Quantum yields for bpH<sup>•</sup>Tyr(O<sup>•</sup>) formation,  $\Phi_{BR}$  (Table 2), are extracted from the concentration profiles in Figure 13 by extrapolation back to the end of the excitation pulse. These quantum yields for **1c,d** in CH<sub>3</sub>CN are not different from 1.00 if account is taken for the experimental error, which is estimated to be not smaller than  $\pm 0.05$ . Biradical formation from **1c,d** is generally efficient, irrespective of the solvent (Table 2). The somewhat lower quantum yields observed in MeOH are readily explained by competitive triplet quenching through H-atom abstraction from the solvent [Eq. (7)]. This conclusion follows from the slight non-stoichiometry between bpH<sup>•</sup> and Tyr(O<sup>•</sup>) and from the presence of a long-lived spectral component at 545 nm, identified as bpH<sup>•</sup>. Though quantum yields for biradical formation are close to unity, the dyads **1c,d** are very inert on steady-state irradiation, as inferred from the negligible

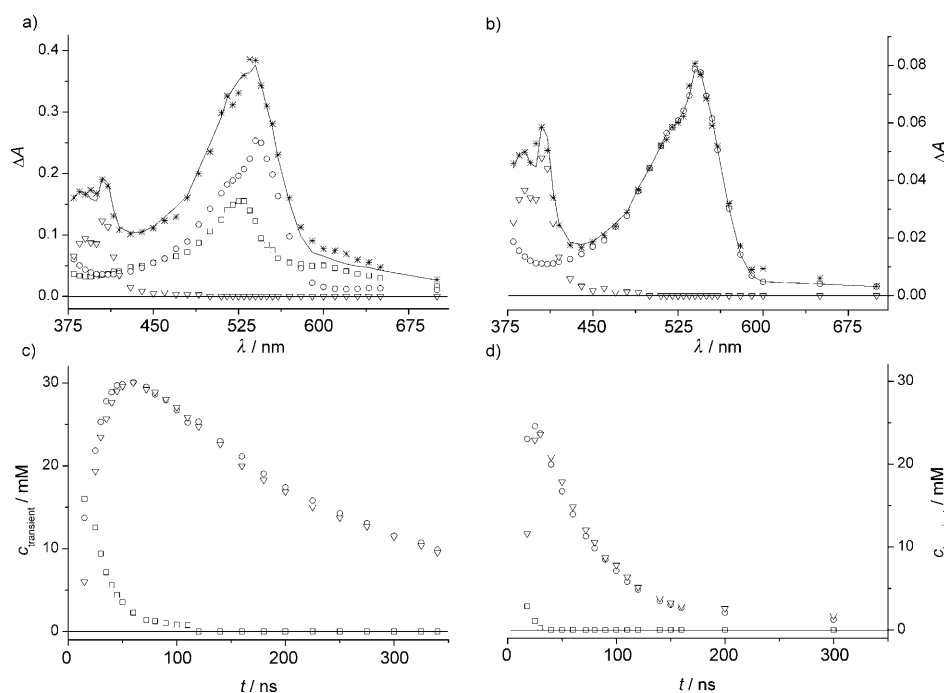


Figure 13. Upper part: Spectral resolutions of transient absorption spectra taken a) 35 ns and b) 400 ns after 355-nm laser pulsing (7 mJ) of a solution of **1c**; in (a) and (b) the squares represent the triplet-state  $^3\text{bp}$ , circles the ketyl radical  $\text{bpH}^\bullet$ , triangles the tyrosyl radical  $\text{Tyr}(\text{O}^\bullet)$ , and \* the experimental data; solid curves are the resulting fits from the regression analysis. Lower part: Concentration profiles for the transients  $^3\text{bp}$  (squares),  $\text{bpH}^\bullet$  (circles), and  $\text{Tyr}(\text{O}^\bullet)$  (triangles), obtained from deconvolution of transient absorption spectra of **1c** and **1d** after delays of 15–350 ns with a concentration  $[\mathbf{1c,d}] = 1.5 \times 10^{-3} \text{ M}$ ; initial triplet concentration  $[\text{T}]_0 = 38 \pm 2 \mu\text{M}$ .

quantum yields for dyad consumption in inert solvents ( $\Phi_{\text{irr}} < 0.01$ ; Table 1). It appears that both triplet quenching and biradical decay are strictly intramolecular reactions at sufficiently low concentrations of starting materials. This type of “reversible” H-atom transfer presents an efficient path for energy dissipation in the triplet-excited bp moiety.

**Effects of molecular geometry on the intramolecular H-atom-transfer rates:** Photochemical and photophysical parameters of aromatic carbonyls have been referred to aspects of molecular geometry before.<sup>[33]</sup> Hydrogen-atom transfer, as a typical reaction of triplet-excited carbonyls, demands close contacts of the reacting units.<sup>[34a]</sup> Remarkable geometrical effects on H-atom transfer in oxyethyl-linked acetophenone–phenol dyads have been reported.<sup>[5c]</sup> In the cited work the substitution pattern of ketone and phenol were systematically varied. Semiempirical (PM3) calculations revealed that the flexible linker allows the formation of possibly reactive exciplexes, irrespective of the substitution pattern. The striking contrast between completely inert and highly active regioisomers was accordingly referred to symmetrical restrictions of electronic overlap of phenol and ketone  $\pi$  systems.

It is appealing to interpret also the reactivity order of the dyads **1a–d** in terms of molecular geometry. Discussion is based on the results of ground-state NMR and molecular-

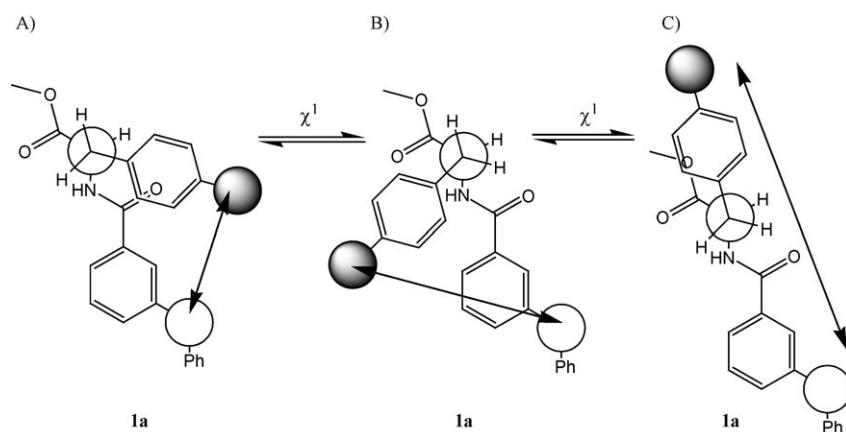
modeling studies (see above), which are assumed to apply also in the triplet-excited state of the dyads. Apparently, the molecular structure of dyads **1c,d** allows reactive contact of the excited triplet state with the remote phenol group of the Tyr residue with high yields (Table 2) in any of the solvents studied. In contrast, the triplet states of the dyads **1a,b** are very inert in  $\text{CH}_3\text{CN}$  or are transformed into  $\text{bpH}^\bullet$  radicals predominantly through H-atom abstraction from the solvent in MeOH. Although **1b** remains inactive towards intramolecular processes also in  $\text{CH}_2\text{Cl}_2$ , **1a** efficiently undergoes intramolecular H-atom transfer to yield biradicals,  $\text{bpH}^\bullet\text{Tyr}(\text{O}^\bullet)$ . Clearly, the approach of the remote reaction sites depends on the geometric constraints on intramolecular motions. The general pattern of intramolecular reactivity,  $k_{\text{H}}(\mathbf{1d}) > k_{\text{H}}(\mathbf{1c}) \gg k_{\text{H}}(\mathbf{1a}) \gg k_{\text{H}}(\mathbf{1b})$ , as found in  $\text{CH}_2\text{Cl}_2$  solution, can be qualitatively rationalized on grounds

of molecular-geometry considerations.

The dyads **1a–d** are expected to be intrinsically less flexible than the dyads in ref. [5c]. This difference can be associated with the chemical nature of the linking group. Oxyalkyl groups, as they were used in the cited work, are known to increase chain flexibility and to favour folded structures.<sup>[34b]</sup> In contrast, the presence of a rigid amide spacer in our dyads decreases the flexibility of the chain, even though the chain is nominally even longer than in the cited work. In addition, the directionality of the amide function renders the distribution of the conformations anisotropic. This situation was already illustrated in Scheme 1b. In that simplified picture, the molecular dynamics were broken down into the space accessible for the Tyr residue by mapping out the angular limits of its amide nitrogen. The predictions from this intuitive picture are fully confirmed by the results from the molecular-dynamics simulations (Figure 7), in which it can be seen that close contacts between the carbonyl and the remote phenol group are not favoured for **1a** and are strictly excluded for **1b**. In the ketoprofen-based dyads **1c,d**, the insertion of an alkyl group between benzophenone and the amide group extends the chain length with respect to **1a,b**. The directionality of the precession cone from **1a** ( $120^\circ$ ) is preserved, however, the additional hinge in **1c,d** greatly extends the opening angle of the cone (Scheme 1b). This anticipated higher flexibility of the **1c,d** dyads is convincingly

reflected in the  $r_{O...O}$  distributions obtained from molecular-dynamics simulations. Already within this simplified approach important qualitative conclusions can be drawn: For **1b**, the geometrical constraints posed by concerted effects of 1) unfavourable directionality of substitution and 2) the lack of intrinsic flexibility of the linker combine to exclude any close contacts between the carbonyl and the phenol functions. Accordingly, **1b** is not able to dissipate the excitation energy by means of intramolecular H-atom transfer. For **1a**, condition (2) is still valid, whereas the change in directionality upon change in substitution (from *para* in **1b** to *meta* in **1a**) allows for the close approach of the reacting groups, at least to some extent (Figure 7).

In addition to effects of the probability of close contacts (Figure 7) the orientation of the reacting moieties may affect the overall reactivity, as was concluded in ref. [5c]. A similar conclusion can be drawn from a discussion of the steric constraints that have to be fulfilled for **1a** to reach a reactive conformation. In Scheme 3, the combined structural



Scheme 3. Interchromophore distances (arrows) of carbonyl (white circle) and hydroxyl (grey circle) moieties in **1a** for the side-chain rotamers g- (A), g+ (B), and t (C).

peculiarities of the benzamide group and of the peptide backbone greatly confine the possible conformations in the dyad **1a**. 1) An extended conformation of the peptide backbone is strongly favored, as was concluded from the high NH-H $\alpha$  coupling constants in  $^1\text{H}$  NMR. The amide function, C(O)-NH, and the C $\alpha$ -C(O) group are almost co-planar. 2) In addition, the amide group of *N*-methyl-benzamide has been reported to be tilted from co-planarity with the phenyl  $\pi$  system by a well-defined angle of 20 $^\circ$ .<sup>[35]</sup>

The consequences of rotation around  $\chi^1$  in the Tyr side chain in **1a** for the distance between the phenol (grey circle) and the carbonyl (white circle) are illustrated in Scheme 3 (for the sake of visual clarity the small deviations from co-planarity of the *N*-benzoyl amide and the peptide backbone are neglected). The given situation affords close contacts between the phenol and the carbonyl only in the rotamer state g- (structure **1a**, A) in Scheme 3). Alternatively, the structure **1a**, B) yields close contacts after rotation by 180 $^\circ$  about

the phenyl-C(O) bond (not shown). Thus, only a minor fraction of the molecules occupies conformations that are reactive for H-atom transfer between hydroxyl and carbonyl groups (Figure 7 and Scheme 3). However, triplet-excitation of the dyad **1a** yields the biradical BR with unity quantum yield in CH<sub>2</sub>Cl<sub>2</sub> (Table 2). It is concluded that the conformational exchange between the active and unreactive rotamers occurs on a timescale faster than the intrinsic triplet decay [Eq. (6)]. This finding is in agreement with the results obtained in similar systems.<sup>[5a,b]</sup>

Importantly, neither of the two possibly reactive conformations of **1a** allow for significant enough overlap of the  $\pi$  systems of Tyr and bp in order to form exciplexes. This is in accord with the negligible ring-current effects on the aromatic Tyr protons of **1a** (Figures 4 and 5). Vice versa, the higher reactivity of the alkylamides **1c,d** (and their reactivity order,  $k_{\text{H}}(\textbf{1d}) > k_{\text{H}}(\textbf{1c})$ ) corresponds to significant ground-state interactions between the aromatic moieties. Because exciplexes have been commonly proposed to be

crucial intermediates of H-atom transfer in the ketone/phenol system,<sup>[5a-d, 6a, d, e, 7a, d]</sup> we conclude that the low rate constants of **1a** (relative to **1c,d**) are a consequence of the missing overlap between the  $\pi$  systems of Tyr and bp.

*Intramolecular H-atom transfer—Media effects:* It can be inferred from an inspection of Table 2 that the rate constants for triplet decay,  $k_{\text{d}}$ , and, concomitantly, the rate constants for intramolecular H-atom transfer,  $k_{\text{H}}$ , of **1a** and **1c** are dependent on the reaction medium. In contrast, the H-atom-transfer rate constants of

**1d** vary only slightly upon going from CH<sub>2</sub>Cl<sub>2</sub> to MeOH solutions. Generally, the highest rates are observed in non-polar solvents such as CH<sub>2</sub>Cl<sub>2</sub>. This might be attributed to favourable conditions towards H-atom transfer being present in solvents of lower “polarity”. This is corroborated by the observation of highly reactive triplet states of **1c,d** in benzene and chloroform, or of **1a** in *n*-butylchloride.<sup>[36]</sup> A general result from related studies appears to be that there is a correlation between the rate constants and the H-bonding properties of the solvents. In particular, the commonly observed decrease of H-atom-transfer reactivity as HB-acceptor ability increases is interpreted as being due to a reduction in the concentration of free phenol by hydrogen bonding to the solvent.<sup>[37]</sup> The concept of a solvent-dependent “masking” of the phenol was recently applied to the qualitative<sup>[6b, 7a, 38]</sup> and quantitative<sup>[7f]</sup> analysis of the solvent dependence of the triplet quenching by phenols. The observed proportionality between the chemical shifts of the



phenolic protons and the HB-acceptor ability of the solvents (see above) supplies direct evidence for an H-bonding equilibrium also for the dyads **1a–d**.

Our results are qualitatively in accord with the results of the cited studies in that we observe a decrease in the rate constants as HB-acceptor ability of the solvent increases. However, the extent of the kinetic solvent effect (KSE) appears to be strongly dependent on the dyad structures. The KSE that was observed for **1a** strongly exceeds the ones for **1c** and especially for **1d**. This contradicts the model that predicts uniform KSEs, expressed as the slopes in linear plots of  $\log k_{\text{H}}$  versus  $\beta_2^{\text{H}}$ , for a uniform H-atom donor (here: phenol). Interestingly, the observed order in KSEs ( $\text{KSE}(\mathbf{1d}) < \text{KSE}(\mathbf{1c}) \ll \text{KSE}(\mathbf{1a})$ ) appears to mirror the order of ground-state interactions between the aromatic Tyr and bp moieties, which were derived from the ring-current effects on the Tyr resonances (Figures 4 and 5). Variations in the solvent dependencies are indicative of structure-specific deviations from the assumptions of the Ingold model. A possible correlation between the dyad structure and the KSE serves as the working hypothesis for ongoing work that addresses the solvent dependencies of H-atom transfer in bp/Tyr dyads in further detail.<sup>[36]</sup>

## Conclusion

Hydrogen-atom transfer in the triplet-excited  $n \rightarrow \pi^*$  state of bp/Tyr dyads is a prominent pathway of intramolecular triplet-energy dissipation. As the formation of reactive head-to-tail contacts between the remote groups requires intramolecular motions, it is expected to be modulated by the nature of the linker. In fact, the H-atom-transfer efficiencies of the dyads in this study depend markedly on the dyad structure and the reaction medium. In this study we have identified molecular parameters that control the overall rates and efficiencies of the intramolecular reaction. In a given solvent the directionality of and the flexibility within the amide-type linker are selectors of the distance and the orientation of the interacting moieties. A qualitative order of reactivity has been established based on geometrical considerations, NMR investigations, and molecular-dynamics simulations, which address the distance distributions and relative orientations between the reacting groups as a function of the molecular structure.

Within a series of three dyads (**1a** and **1c,d**) that differ solely in the nature of the amide-linking group between the phenol and the triplet-excited ketone, the efficiency of the reactive approach can be correlated with the probability of close contacts and the extent of electronic overlap. Geometrically restricted overlap, as evidenced by insignificant aromatic–aromatic interactions in the benzamide **1a**, leads to substantially smaller H-atom-transfer rates than in the alkylamides **1c,d**, although similar distance distributions are observed in all three cases. The high reactivity of **1c,d** is paralleled by strong NMR ring-current effects that indicate effective head-to-tail interactions already in the ground state.

This simultaneous dependence on distance and orientation is a strong argument for exciplexes being important intermediates on the H-atom-transfer reaction coordinate, with the stability of the respective exciplex being reflected by the strength of the ground-state ring-current effects.

These results have implications on the interpretation of the chiral discrimination that was reported for H-atom transfer in related dyads.<sup>[6a,c,d]</sup> In the cited work, the stereoselectivity was associated with “nonbonding electronic interactions between the aromatic  $\pi$  systems”,<sup>[6a]</sup> which was suggested to be different for different diastereomers. The argumentation was based mainly on X-ray crystallographic data. In favour of this interpretation given by Miranda et al., the epimeric dyads **1c** and **1d** in our study, with (*S*) and (*R*)-configuration of the Tyr moieties, respectively, exhibit stereoselectivity in the H-atom-transfer rates and in the probability of ground-state head-to-tail contacts. Thus, it is appealing to interpret the stereoselectivity in excited-state reactivity as a consequence of sterically controlled electronic overlap between the aromatic moieties.

## Experimental Section

**General:** Routine  $^1\text{H}$  and  $^{13}\text{C}$  NMR spectra (200/500 MHz and 50.32 MHz, respectively) were recorded in deuterated solvents. Chemical shifts  $\delta$  are reported in ppm downfield from TMS (experimental error:  $\Delta\delta \pm 0.01$  ppm). Assignment of resonances was based on  $^1\text{H}$ – $^1\text{H}$  and  $^1\text{H}$ – $^{13}\text{C}$  COSY spectra. Parameters of the 1D-NOE measurements for **1a** and **1c,d** in  $\text{CDCl}_3$  and  $\text{CD}_3\text{CN}$  (500 MHz): double PFG spin-echo (DPFGSE)-NOE sequence,<sup>[39]</sup> spectral width 4390 Hz, 16 k complex data points, 2880 scans per irradiation point, acquisition time 3.7 s, relaxation delay 2.0 s, NOE-buildup delay 500 ms, gradient strengths 14/6/4/–4 % ( $100\% = 140 \text{ G cm}^{-1}$ ), gradient duration 1 ms each, selective Gauss pulse 40 ms, exponential line broadening with BF = 1.0 Hz.

UV/Vis spectra were recorded by using a Varian Cary 300 Bio UV-visible spectrophotometer in  $10^{-6}$  to  $10^{-5}$  molar concentrations. Millimolar concentrations were employed for the determination of the  $n \rightarrow \pi^*$  transitions of benzophenone chromophores around 340 nm. Phosphorescence emission and excitation spectra and phosphorescence decays were recorded by using a Spex FluoroMax-P (Horiba Jobin Yvon) in acetonitrile and a Perkin–Elmer LS 50B in MeOH/EtOH 1:1 glass at an excitation wavelength of 330 nm at 77 K. Concentrations were set in the millimolar range, corresponding to absorbances *A* at 330 nm of 0.3–0.5.

Steady-state experiments were carried out in 1-cm  $\times$  1-cm rectangular UV cells on standard optical-bench systems. A high-pressure mercury lamp HBO 200 (Narva) together with water filter, quartz windows, interference filter (313 nm), and cut-off glass filters ( $< 290$  nm) were used as the excitation source for 313 nm irradiations. A low-pressure mercury lamp (Original Hanau TNN 15/30) was used as the excitation source for the 254 nm irradiation. Reaction progress was monitored by UV/Vis spectroscopy with a HP Diode Array 8452A Spectrophotometer or by HPLC using a Waters 600E Multisolute Delivery System Pump, as described previously.<sup>[40]</sup> The detection system consisted of a Waters 996 Photodiode Array UV/Vis Detector. Analytical HPLC analyses were carried out on a Waters XTerra RP<sub>18</sub> reverse phase column (4.6  $\times$  250 mm, 5-mm particle size). Uranyl oxalate actinometry was used to measure the light intensity. The quantum yields for this actinometry were taken to be 0.602 and 0.561 for the 254 and 313 nm irradiations, respectively.<sup>[30]</sup> Light flux was within the range of  $10^{-4} \text{ Einstein dm}^{-2} \text{ min}^{-1}$  at both wavelengths.

The equipment for laser flash photolysis has been described in detail previously.<sup>[41]</sup> It is based on the 266 or 355 nm output of a Nd/YAG laser with a full width at half maximum of approximately 7 or 9 ns and a dose



of 5-mJ pulse<sup>-1</sup> or 7-mJ pulse<sup>-1</sup>, respectively. Transient decays were recorded at individual wavelengths by the step-scan method with a step distance of 5 nm in the range of 300 to 800 nm and obtained as the mean signals of 6 to 16 pulses. Spectral resolution was in the range of  $\pm 3$  nm. Samples for LFP were rigorously deoxygenated by flushing with analytical-grade nitrogen in a circulating flow system (5  $\times$  5-mm Suprasil quartz cell) for 20 min prior to and kept under nitrogen during measurement.

**Synthesis:** Chemicals and solvents (Sigma–Aldrich and BACHEM) for synthesis were of highest available analytical grade and were used without further purification. Synthesis of the dyads followed the routines of carbodiimide-induced amide-coupling (for details of procedures and characterization, see Supporting Information). The identity and purity of the dyads were studied by <sup>1</sup>H and <sup>13</sup>C NMR and combustion analysis. The obtained NMR spectra were in accord with the molecular structures of **1a–d**. Combustion analysis gave slight deviations from ideal stoichiometry for the benzamide **1b** due to inclusion of residual solvent (diethyl ether, ethyl acetate) in the crystalline foams, which could not be removed even on extended evacuation. Attempts to produce the dyads as crystalline material were not successful. However, because HPLC analysis proved the absence of contaminants absorbing light with  $\lambda > 220$  nm in all cases, the dyads were used in this study without further work-up.

**Spectral analysis of LFP intermediates:** Quantum yields for the formation of the *i*th transient,  $\Phi_i$ , were obtained by using relative actinometry with benzophenone solutions of matched optical density in acetonitrile, CH<sub>3</sub>CN [Eq. (12)]. The absorbed light intensity  $I_a$  is expressed as the resulting triplet-state concentration in the actinometer solution with the measured  $\Delta A_T$  at 525 nm. The known values of molar absorption coefficient  $\epsilon_T(525 \text{ nm}) = 6500 \text{ M}^{-1} \text{ cm}^{-1}$  and triplet quantum yield  $\Phi_T(\text{bp}) = 1.00$  were also used in Equation (12).<sup>[31]</sup>

$$\Phi_i = \frac{c_i}{I_a} = \frac{\Delta A(\lambda_i)}{\epsilon(\lambda_i)} \times \frac{\Phi_T(\text{bp}) \times \epsilon_T(525 \text{ nm})}{\Delta A_T(525 \text{ nm})} \quad (12)$$

Here,  $\Delta A(\lambda_i)$  and  $\epsilon(\lambda_i)$  denote the measured change in optical density after laser pulsing of the sample solution, and the molar absorption coefficient of the transient at the wavelength  $\lambda_i$ , respectively. The procedure summarized in Equation (12) is limited to cases in which wavelengths exist that are characteristic for a single transient. In the more common case of convoluted spectra, a multi-regression analysis has to be done on the optical transient spectra resulting from pulsed irradiation in order to extract the individual transient concentrations  $c_i$ . Within any time window, following the excitation pulse, the absorbance of the signal is related to the concentrations and molar absorption coefficients of the transients through Beers Law  $\Delta A = \log(I_0/I)$ .

$$\Delta A(\lambda_i) = \sum_{i=1}^n c_i \times \epsilon_i(\lambda_i) \times l \quad (13)$$

In the regression analysis of the experimental spectra by Equation (13) the concentrations of the individual transients times the optical path-length,  $l \times c_i$ , are the regression parameters to be fit.<sup>[42]</sup> The sets of  $\epsilon_i(\lambda_i)$  are the reference spectra of the underlying transients enumerated by the *i*-th subscript. The uncertainties for the  $c_i$  are computed from the square roots of the diagonal matrix elements of the covariance matrix for each linear regression.

Reference spectra for the excited triplet states of the bp∪Tyr dyads **1a–d** were obtained by LFP of diluted solutions of the model compounds **2a–c** in CH<sub>3</sub>CN and dichloromethane, CH<sub>2</sub>Cl<sub>2</sub>. Molar absorption coefficients were obtained by comparison of the transient absorptions  $\Delta A(\lambda_{\text{max}})$  and  $\Delta A_T(525 \text{ nm})$  of the actinometer solution at time delays for which no significant decay has taken place, and under the assumption of unity triplet yield.<sup>[31]</sup> Spectra of radical species relevant to this study were obtained by bimolecular quenching of the respective triplet states of **2a–c** in CH<sub>3</sub>CN with methanol, MeOH, or 2-propanol. Spectra of the resulting ketyl radicals (bpH<sup>•</sup>; also: hemipinacol) were corrected by scaling with known molar absorption coefficients. Because ketyl anion radicals (bp<sup>•-</sup>) turned out to be of minor importance in this study, no attempts were made to establish a set of reference spectra for these species. If needed, a literature-

known spectrum of bp<sup>•-</sup> was used in the regression.<sup>[43]</sup> The tyrosyl radical Tyr(O<sup>•</sup>) was represented in the regression analysis by a spectrum measured in water by pulse radiolysis.<sup>[44a]</sup> The LFP spectra in our study were recorded at substantially lower resolution, which leads to dampening of the very narrow absorption feature of Tyr(O<sup>•</sup>) at 405 nm. Thus, the molar absorption coefficient reported in the cited work for Tyr(O<sup>•</sup>) ( $\epsilon_{\text{Tyr}}(405 \text{ nm}) = 3200 \text{ M}^{-1} \text{ cm}^{-1}$ ) appeared to be inadequate. A value of  $\epsilon_{\text{Tyr}}(405 \text{ nm}) = 1900 \text{ M}^{-1} \text{ cm}^{-1}$  for acetonitrile solution, which is in accord with literature data for a protein-bound Tyr(O<sup>•</sup>),<sup>[44b]</sup> was extracted from bimolecular quenching experiments of bp with *N*-Boc-Tyr-OMe, based on equimolar formation of Tyr(O<sup>•</sup>) and bpH<sup>•</sup>.

**Computational methods:** The statistical distribution of the distances (pair-distribution function),  $r_{\text{O} \cdots \text{O}}$ , between the carbonyl oxygen atom of the bp moiety and the Tyr hydroxylic oxygen was calculated from the potential of mean force,  $w(r_{\text{O} \cdots \text{O}})$ , by using Equation (14).<sup>[45]</sup>

$$g(r_{\text{O} \cdots \text{O}}) = \exp\{-w(r_{\text{O} \cdots \text{O}})/k_B T\} \quad (14)$$

These calculations were accomplished with umbrella sampling,<sup>[46]</sup> done in conjunction with Langevin dynamics (LD)<sup>[47–49]</sup> and the CHARMM<sup>[50]</sup> all-atom empirical potential. In the LD no explicit solvent molecules were used, but the usual LD frictional drag of the solvent was factored in by using a collision frequency for all heavy atoms equal to approximately 20 ps<sup>-1</sup>, which reflects the viscosity of acetonitrile. We set the sampling windows at intervals of 0.1 Å and a force constant for the umbrella potential of 20 kcal mol<sup>-1</sup> Å<sup>-2</sup> (83.7 kJ mol<sup>-1</sup> Å<sup>-2</sup>). Each window simulation was run with a 1.5-fs time step for 50 ps, preceded by 9 ps of heating from 0 to 300 K and 10 ps of equilibration. For the CHARMM27 force-field calculations, we used version 7 of the HyperChem PC molecular-modeling package.<sup>[51]</sup> To suppress unrealistic over-representation (see above) of short distances,  $r_{\text{O} \cdots \text{O}}$ , with carbonyl and hydroxyl in hydrogen bonding, the atom charges of all the atoms of the molecules were set to zero which, in practice, is the equivalent of setting the dielectric permittivity equal to infinity.

## Acknowledgements

This work was supported by the Research Training Network SULFRAD (HPRN-CT-2002-00184) and by COST Chemistry CM0603. The authors thank Prof. O. Brede and Dr. R. Hermann (University Leipzig, Germany) for access to the LFP equipment and for technical support. The computation was performed employing the computation resources of the Interdisciplinary Centre for Mathematical and Computation Modelling of the Warsaw University (G-24-13) and the Albigowa Biotechnology Centre of the Rzeszow University of Technology. This paper is Document No. NDRL-4751 from the Notre Dame Radiation Laboratory. G.L.H. was a Fulbright Scholar at AMU.

- [1] a) J. Stubbe, W. A. van der Donk, *Chem. Rev.* **1998**, 98, 705–762; b) C. W. Hoganson, C. Tommos, *Biochim. Biophys. Acta* **2004**, 1655, 116–122.
- [2] For representative examples, see: a) G. W. Burton, K. U. Ingold, *Acc. Chem. Res.* **1986**, 19, 194–201; b) C. Evans, J. C. Scaiano, K. U. Ingold, *J. Am. Chem. Soc.* **1992**, 114, 4589–4593; c) J. M. Mayer, D. A. Hrovat, J. L. Thomas, W. T. Borden, *J. Am. Chem. Soc.* **2002**, 124, 11142–11147; d) M. Sjödin, S. Styring, H. Wolpher, Y. Xu, L. Sun, L. Hammarström, *J. Am. Chem. Soc.* **2005**, 127, 3855–3863; e) I. J. Rhile, T. F. Markle, H. Nagao, A. G. DiPasquale, O. P. Lam, M. A. Lockwood, J. M. Mayer, *J. Am. Chem. Soc.* **2006**, 128, 6075–6088; f) O. Brede, S. Naumov, *J. Phys. Chem. A* **2006**, 110, 11906–11918; g) M. Sjödin, T. Irebo, J. E. Utas, J. Lind, G. Merenyi, B. Akermark, L. Hammarström, *J. Am. Chem. Soc.* **2006**, 128, 13076–13083; h) F. Thomas, O. Jarjays, H. Jamet, S. Hamman, E. Saint-Aman, C. Duboc, J.-L. Pierre, *Angew. Chem.* **2004**, 116, 604–607; *Angew. Chem. Int. Ed.* **2004**, 43, 594–597.

- [3] P. K. Das, M. V. Encinas, S. Steenken, J. C. Scaiano, *J. Am. Chem. Soc.* **1981**, *103*, 4162–4166.
- [4] P. K. Das, M. V. Encinas, J. C. Scaiano, *J. Am. Chem. Soc.* **1981**, *103*, 4154–4162.
- [5] a) J. C. Scaiano, W. G. McGimpsey, W. J. Leigh, S. Jakobs, *J. Org. Chem.* **1987**, *52*, 4540–4544; b) W. J. Leigh, E. C. Lathioor, M. J. St. Pierre, *J. Am. Chem. Soc.* **1996**, *118*, 12339–12349; c) E. C. Lathioor, W. J. Leigh, M. J. St. Pierre, *J. Am. Chem. Soc.* **1999**, *121*, 11984–11992; d) E. C. Lathioor, W. J. Leigh, *Can. J. Chem.* **2001**, *79*, 1851; e) E. C. Lathioor, W. J. Leigh, *Photochem. Photobiol.* **2006**, *82*, 291–300.
- [6] a) M. A. Miranda, A. Lahoz, R. Martinez-Manez, F. Bosca, J. V. Castell, J. Perez-Prieto, *J. Am. Chem. Soc.* **1999**, *121*, 11569–11570; b) J. Perez-Prieto, F. Bosca, R. E. Galian, A. Lahoz, L. R. Domingo, M. A. Miranda, *J. Org. Chem.* **2003**, *68*, 5104–5113; c) J. Perez-Prieto, A. Lahoz, F. Bosca, R. Martinez-Manez, M. A. Miranda, *J. Org. Chem.* **2004**, *69*, 374–381; d) J. Perez-Prieto, S.-E. Stiriba, F. Bosca, A. Lahoz, L. R. Domingo, F. Mourabit, S. Monti, M. A. Miranda, *J. Org. Chem.* **2004**, *69*, 8618–8625; e) J. Perez-Prieto, R. E. Galian, M. C. Morant-Mirana, M. A. Miranda, *Chem. Commun.* **2005**, 3180–3182; f) R. E. Galian, L. Pastor-Perez, M. A. Miranda, J. Perez-Prieto, *Chem. Eur. J.* **2005**, *11*, 3443–3448.
- [7] a) L. Biczok, T. Berces, H. Linschitz, *J. Am. Chem. Soc.* **1997**, *119*, 11071–11077; b) U. Pischel, W. M. Nau, *Photochem. Photobiol. Sci.* **2002**, *1*, 141–147; c) M. Yamaji, Y. Aoyama, T. Furukawa, T. Ito, S. Tobita, *Chem. Phys. Lett.* **2006**, *420*, 187–191; d) U. Pischel, D. Patra, A. L. Koner, W. M. Nau, *Photochem. Photobiol.* **2006**, *82*, 310–317; e) M. R. Seyedsayamdost, S. Y. Reece, D. G. Nocera, J. Stubbe, *J. Am. Chem. Soc.* **2006**, *128*, 1569–1579; f) R. E. Galian, G. Litwinienko, J. Perez-Prieto, K. U. Ingold, *J. Am. Chem. Soc.* **2007**, *129*, 9280–9281.
- [8] N. J. Turro, R. Engel, *J. Am. Chem. Soc.* **1969**, *91*, 7113–7121.
- [9] a) S. Canonica, B. Hellrung, J. Wirz, *J. Phys. Chem. A* **2000**, *104*, 1226–1233; b) N. B. Sultimova, P. P. Levin, O. N. Chaikovskaya, *Russ. Chem. Bull.* **2005**, *54*, 1439–1444.
- [10] M. P. Williamson, J. P. Waltho, *Chem. Soc. Rev.* **1992**, *21*, 227–236.
- [11] M. Karplus, *J. Chem. Phys.* **1959**, *30*, 11–15.
- [12] M. Kraszni, Z. Skakacs, B. Noszal, *Anal. Bioanal. Chem.* **2004**, *378*, 1449–1463.
- [13] R. L. Laws, J. B. A. Ross, H. R. Wyssbrod, J. M. Beechem, L. Brand, J. C. Sutherland, *Biochemistry* **1986**, *25*, 599–607.
- [14] G. W. Kirby, J. Michael, *J. Chem. Soc. D* **1971**, 187–188.
- [15] K. G. R. Pachler, *Spectrochim. Acta* **1964**, *20*, 581–587.
- [16] J. R. Unruh, M. R. Liyanage, C. K. Johnson, *J. Phys. Chem. B* **2007**, *111*, 5494–5502.
- [17] C. Reichardt, *Solvents and Solvent Effects in Organic Chemistry*, 2nd ed., VCH, Weinheim, **1990**, p. 408.
- [18] a) J. Kobayashi, U. Nagai, *Biopolymers* **1978**, *17*, 2265–2277; b) J. Kobayashi, T. Higashijima, S. Sekido, T. Miyazawa, *Int. J. Peptide Protein Res.* **1981**, *17*, 486–494; c) J. Kobayashi, T. Higashijima, T. Miyazawa, *Int. J. Peptide Protein Res.* **1984**, *24*, 40–47.
- [19] J. B. A. Ross, W. R. Laws, A. Buku, J. C. Sutherland, H. R. Wyssbrod, *Biochemistry* **1986**, *25*, 607–612.
- [20] a) M. Kainosho, K. Ajskovic, *J. Am. Chem. Soc.* **1975**, *97*, 5630–5631; b) K. Guzow, R. Ganzynkowicz, A. Rzeska, J. Mrozek, M. Szabelski, J. Karolczak, A. Liwo, W. Wicz, *J. Phys. Chem. B* **2004**, *108*, 3879–3889.
- [21] G. Scherer, M. L. Kramer, M. Schutkowski, U. Reimer, G. Fischer, *J. Am. Chem. Soc.* **1998**, *120*, 5568–5574.
- [22] R. W. Taft, M. J. Kamlet, *Org. Magn. Reson.* **1980**, *14*, 485–493.
- [23] a) T. Steiner, *Angew. Chem.* **2002**, *114*, 50–80; *Angew. Chem. Int. Ed.* **2002**, *41*, 48–76; b) G. Jaccard, J. Lauterwein, *Helv. Chim. Acta* **1986**, *69*, 1469–1485.
- [24] J. Koput, G. Hörner, F. Kazmierczak, B. Marciniak, unpublished results.
- [25] a) E. A. Meyer, R. K. Castellano, F. Diederich, *Angew. Chem.* **2003**, *115*, 1244–1287; *Angew. Chem. Int. Ed.* **2003**, *42*, 1210–1250; b) R. Chelli, F. L. Gervasio, P. Procacci, V. Schettino, *J. Am. Chem. Soc.* **2002**, *124*, 6133–6143.
- [26] a) M. Sheinblatt, *J. Chem. Soc. Perkin Trans. 2* **1990**, 127–132; b) R. Mahalakshmi, S. Raghothama, P. Balaram, *J. Am. Chem. Soc.* **2006**, *128*, 1125–1138.
- [27] V. Rizzo, H. Jäckle, *J. Am. Chem. Soc.* **1983**, *105*, 4195–4205.
- [28] M. H. Abraham, P. L. Grellier, D. V. Prior, J. J. Morris, P. J. Taylor, *J. Chem. Soc. Perkin Trans. 2* **1990**, 521–529.
- [29] N. J. Turro, *Modern Molecular Photochemistry*, University Science Books, CA, USA, **1991**.
- [30] S. L. Murov, I. Carmichael, G. L. Hug, *Handbook of Photochemistry*, Marcel Dekker, New York, **1993**.
- [31] R. V. Bensasson, J.-C. Gramain, *J. Chem. Soc. Faraday Trans. 1* **1980**, *76*, 1801–1810.
- [32] T. Kluge, O. Brede, *Chem. Phys. Lett.* **1998**, *289*, 319–323.
- [33] P. J. Wagner, *Acc. Chem. Res.* **1983**, *16*, 461–467.
- [34] a) P. J. Wagner, R. Pabon, B.-S. Park, A. R. Zand, D. L. Ward, *J. Am. Chem. Soc.* **1994**, *116*, 589–596; b) P. J. Wagner, P. Klan, *J. Am. Chem. Soc.* **1999**, *121*, 9626–9635.
- [35] R. Vargas, J. Garza, D. Dixon, B. P. Hay, *J. Phys. Chem. A* **2001**, *105*, 774–778.
- [36] G. Hörner, G. L. Hug, D. Pogocki, B. Marciniak, unpublished results.
- [37] a) D. W. Snelgrove, J. Luszytyk, J. T. Banks, P. Mulder, K. U. Ingold, *J. Am. Chem. Soc.* **2001**, *123*, 469–477; b) G. Litwinienko, K. U. Ingold, *J. Org. Chem.* **2003**, *68*, 3433–3438; c) G. Litwinienko, K. U. Ingold, *J. Org. Chem.* **2004**, *69*, 5888–5896; d) G. Litwinienko, K. U. Ingold, *J. Org. Chem.* **2005**, *70*, 8982–8990; e) G. Litwinienko, K. U. Ingold, *Acc. Chem. Res.* **2007**, *40*, 222–230.
- [38] A. L. Koner, U. Pischel, W. M. Nau, *Org. Lett.* **2007**, *9*, 2899–2902.
- [39] a) S. Braun, H.-O. Kalinowski, S. Berger, *150 and More Basic NMR Experiments*, Wiley-VCH, Weinheim, **1998**, p. 460; b) K. Stott, J. Keeler, Q. N. Van, A. J. Shaka, *J. Magn. Reson.* **1997**, *125*, 302–324.
- [40] P. Filipiak, G. L. Hug, K. Bobrowski, B. Marciniak, *J. Photochem. Photobiol. A* **2005**, *172*, 322–330.
- [41] a) R. Hermann, G. R. Mahalakshmi, S. Jochum, S. Naumov, O. Brede, *J. Phys. Chem. A* **2002**, *106*, 2379–2389; b) O. Brede, T. Leichtner, S. Kapoor, S. Naumov, R. Hermann, *Chem. Phys. Lett.* **2002**, *366*, 377–382.
- [42] P. Wisniowski, G. L. Hug, J. Mirkowski, *DECOM2006*, Warsaw, **2006**.
- [43] E. Hayon, T. Ibata, N. N. Lichtin, M. Simic, *J. Phys. Chem.* **1972**, *76*, 2072–2078.
- [44] a) K. M. Bansal, R. W. Fessenden, *Radiat. Res.* **1976**, *67*, 1–8; b) M. Fontecave, P. Nordlund, H. Eklund, P. Reichardt, *Adv. Enzymol. Relat. Areas Mol. Biol.* **1992**, *65*, 147–183.
- [45] J. G. Kirkwood, *J. Chem. Phys.* **1935**, *3*, 300–313.
- [46] G. M. Torrie, J. P. Valleau, *J. Comp. Physiol.* **1977**, *23*, 187–199.
- [47] R. M. Levy, M. Karplus, J. A. McCammon, *Chem. Phys. Lett.* **1979**, *65*, 4–11.
- [48] G. Widmalm, R. W. Pastor, *J. Chem. Soc. Faraday Trans.* **1992**, *88*, 1747–1754.
- [49] S. He, H. A. Scheraga, *J. Chem. Phys.* **1998**, *108*, 287–300.
- [50] A. D. MacKerell Jr., D. Bashford, R. L. Bellott, R. L. Dunbrack Jr., J. D. Evanseck, M. J. Field, S. Fischer, J. Gao, H. Guo, S. Ha, D. Joseph-McCarthy, L. Kuchnir, K. Kucera, F. T. K. Lau, C. Mattos, S. Michnick, T. Ngo, D. T. Nguyen, B. Prodhom, W. W. Reiher III, B. Roux, M. Schlenkrich, J. C. Smith, R. Stote, J. Straub, M. Watanabe, J. Wiorkiewicz-Kuczera, D. Yin, M. Karplus, *J. Phys. Chem. B* **1998**, *102*, 3586–3616.
- [51] *HyperChem Computational Chemistry*, Hypercube Inc., Gainesville, USA, **2002**.

Received: February 20, 2008  
Published online: July 11, 2008